TABLE I. ***gpt* Mutation Spectra in the Epidermis of UVB-Irradiated *p53*$^{+/+}$ *gpt* Delta Mice**

	0 kJ/m^2		0.5 kJ/m^2		1.0 kJ/m^2		2.0 kJ/m^2	
	No.	MF[a] ($\times 10^{-6}$)	No.	MF ($\times 10^{-6}$)	No.	MF ($\times 10^{-6}$)	No.	MF ($\times 10^{-6}$)
Base substitution								
Transition								
G:C → A:T	24 (6)	6.2	28 (3)	66.1	22 (2)	66.0	28 (3)	66.9
A:T → G:C	1	0.3	0	0.0	2	6.0	1	2.4
Transversion								
G:C → T:A	6	1.6	2	4.7	0	0.0	2	4.8
G:C → C:G	1	0.3	1	2.4	0	0.0	0	0.0
A:T → T:A	2	0.5	3	7.1	3	9.0	2	4.8
A:T → C:G	0	0.0	0	0.0	1	3.0	1	2.4
Tandem base substitution	0	0.0	1	2.4	1	3.0	3	7.2
Deletion	1	0.3	0	0.0	0	0.0	1	2.4
−1 bp	0		0		0		1	
>2 bp	1		0		0		0	
Insertion	0	0.5	0	0.0	0	0.0	0	0.0
Others[b]	0	0.0	1	2.4	0	0.0	0	0.0
Total no.	37	9.6	36	85.0	29	87.0	38	90.9

[a]MFs are calculated by dividing total MF by the ratio of each type of mutations.
[b]Others: TAA to AAG.
( )=CpG sites.

TABLE II. ***gpt* Mutation Spectra in the Epidermis of UVB-Irradiated *p53*$^{-/-}$ *gpt* Delta Mice**

	0 kJ/m^2		0.5 kJ/m^2		1.0 kJ/m^2		2.0 kJ/m^2	
	No.	MF[a] ($\times 10^{-6}$)	No.	MF ($\times 10^{-6}$)	No.	MF ($\times 10^{-6}$)	No.	MF ($\times 10^{-6}$)
Base substitution								
Transition								
G:C → A:T	13 (1)	4.5	22 (2)	54.9	29 (4)	74.6	20	63.1
A:T → G:C	0	0.0	4	10.0	1	2.6	0	0.0
Transversion								
G:C → T:A	1	0.3	0	0.0	0	0.0	4	12.6
G:C → C:G	0	0.0	0	0.0	1	2.6	0	0.0
A:T → T:A	2	0.7	2	5.0	1	2.6	2	6.3
A:T → C:G	0	0.0	2	5.0	1	2.6	0	0.0
Tandem base substitution	2	0.7	3	7.5	1	2.6	0	0.0
Deletion	0	0.0	0	0.0	1	2.6	1	3.2
−1 bp	0		0		1		1	
>2 bp	0		0		0		0	
Insertion	0	0.0	1	2.5	0	0.0	1	3.2
Others[b]	0	0.0	0	0.0	1	2.6	1	3.2
Total no.	18	6.2	34	84.9	36	92.6	28	91.4

[a]MFs are calculated by dividing total MF by the ratio of each type of mutations.
[b]Others = TCA to TT, CCT to CA.
( )=CpG sites.

Spi$^-$ mutation frequencies of large deletions (greater than 1 kb) and complex (deletion with rearrangement) types are shown in Figure 2. In this study, "complex types" were defined as deletion mutants whose junctions were unable to be identified by PCR and sequencing analyses because of the complex rearrangements. In the *p53*$^{+/+}$ mice, the specific Spi$^-$ mutation frequency increased in a dose-dependent manner ($P = 0.01$ in Cochran–Armitage trend test), and was about five times higher at 2.0 kJ/m^2 (0.93×10^{-6}) than that of the unirradiated mice (0.17×10^{-6}). On the other hand, the specific Spi$^-$ mutation frequency of large deletions in unirradiated *p53*$^{-/-}$ mice was significantly higher than that of unirradiated *p53*$^{+/+}$ mice (1.58×10^{-6} compared with 0.17×10^{-6}, $P = 0.04$ in Dunnett test). No significant increase in the specific Spi$^-$ mutation frequency of large deletions was observed in three irradiated groups of *p53*$^{-/-}$ mice. We identified the size and junctions of 39 Spi$^-$ deletions and summarized the nature of the large deletions (greater than 1 kb) recovered from both *p53*$^{-/+}$ and *p53*$^{-/-}$ mice (Fig. 3). The largest deletion size was −7,094 bp. The identical mutation was recovered multiple times from the

TABLE III. Spi⁻ Mutant Frequency in the Epidermis of UVB-Irradiated *gpt* Delta Mice

UVB (kJ/m^2)	Animal ID	Total population	No. of mutants	MF ($\times 10^{-6}$)	Average	SD
p53$^{+/+}$						
0.0	101	1,569,000	5	3.19	1.96	0.89
	102	3,411,000	4	1.17		
	103	1,506,000	3	1.99		
	104	1,361,500	2	1.47		
0.5	201	1,389,000	5	3.60	4.14	1.79
	202	1,629,000	11	6.75		
	203	2,250,000	6	2.67		
	204	1,131,000	4	3.54		
1.0	301	1,907,000	6	3.15	7.31*	3.98
	302	1,421,500	18	12.66		
	303	1,158,000	7	6.04		
	304	1,083,000	8	7.39		
2.0	401	1,038,000	9	8.67	8.24**	0.45
	402	1,800,000	14	7.78		
	403	1,569,000	13	8.29		
	404			ND		
p53$^{-/-}$						
0.0	501	1,735,000	10	5.76	4.91	2.74
	502	714,000	6	8.40		
	503	1,608,000	4	2.49		
	504	1,002,000	3	2.99		
0.5	601	783,000	9	11.49	8.30	2.46
	602	1,005,000	8	7.96		
	603	1,995,000	11	5.51		
	604	1,461,000	12	8.21		
1.0	701	1,344,000	12	8.93	6.04	2.16
	702	1,551,000	9	5.80		
	703	2,442,000	9	3.69		
	704	1,743,000	10	5.74		
2.0	801	1,275,000	15	11.76	8.06	3.47
	803	1,209,000	6	4.96		
	804	1,365,000	14	10.26		
	805	3,048,000	16	5.25		

*Denotes $P < 0.05$ in Dunnett test comparing the MFs of UVB-irradiated versus the corresponding unirradiated mice.
**Denotes $P < 0.01$.

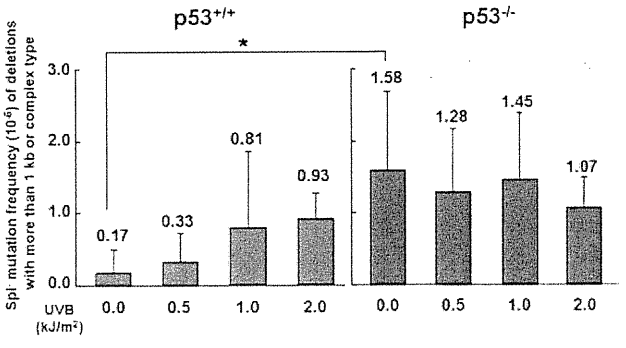

Fig. 2. Specific Spi⁻ mutation frequencies of large deletions (greater than 1 kb) and complex-type deletions in the epidermis of UVB-irradiated *p53*$^{+/+}$ and *p53*$^{-/-}$ *gpt* delta mice. * Denotes $P < 0.05$ ($n = 4$) for the MFs of *p53*$^{-/-}$ mice versus the corresponding *p53*$^{+/+}$ mice (Dunnett test). Vertical bars show the standard deviations with mice as the unit of comparison.

same group: -3,979 bp deletions were recovered from three of four mice for each group (0.5, 1.0, or 2.0 kJ/m^2) of UVB-irradiated *p53*$^{-/-}$ mice. The identical complex type was recovered from four mice with *p53*$^{-/-}$ background irradiated with 1.0 kJ/m^2 UVB.

DISCUSSION

The tumor suppressor gene *p53* plays important roles in the maintenance of genome integrity. To characterize the antimutagenic potential of *p53* in skin carcinogenesis, where *p53* is frequently inactivated by sunlight [Brash et al., 1991], we compared the frequencies and spectra of *gpt* and Spi⁻ mutations in *p53*$^{+/+}$ and *p53*$^{-/-}$ *gpt* delta mice. The *gpt* MFs in the epidermis of *p53*$^{+/+}$ and *p53*$^{-/-}$mice were significantly increased by UVB irradiation at 0.5, 1.0, or 2.0 kJ/m^2 compared with those of unirradiated mice (Fig. 1). However, there were no substantial differences in *gpt* MF between *p53*$^{+/+}$ and *p53*$^{-/-}$ mice. The *gpt* mutation spectra were also similar between *p53*$^{+/+}$ and *p53*$^{-/-}$ mice (Tables

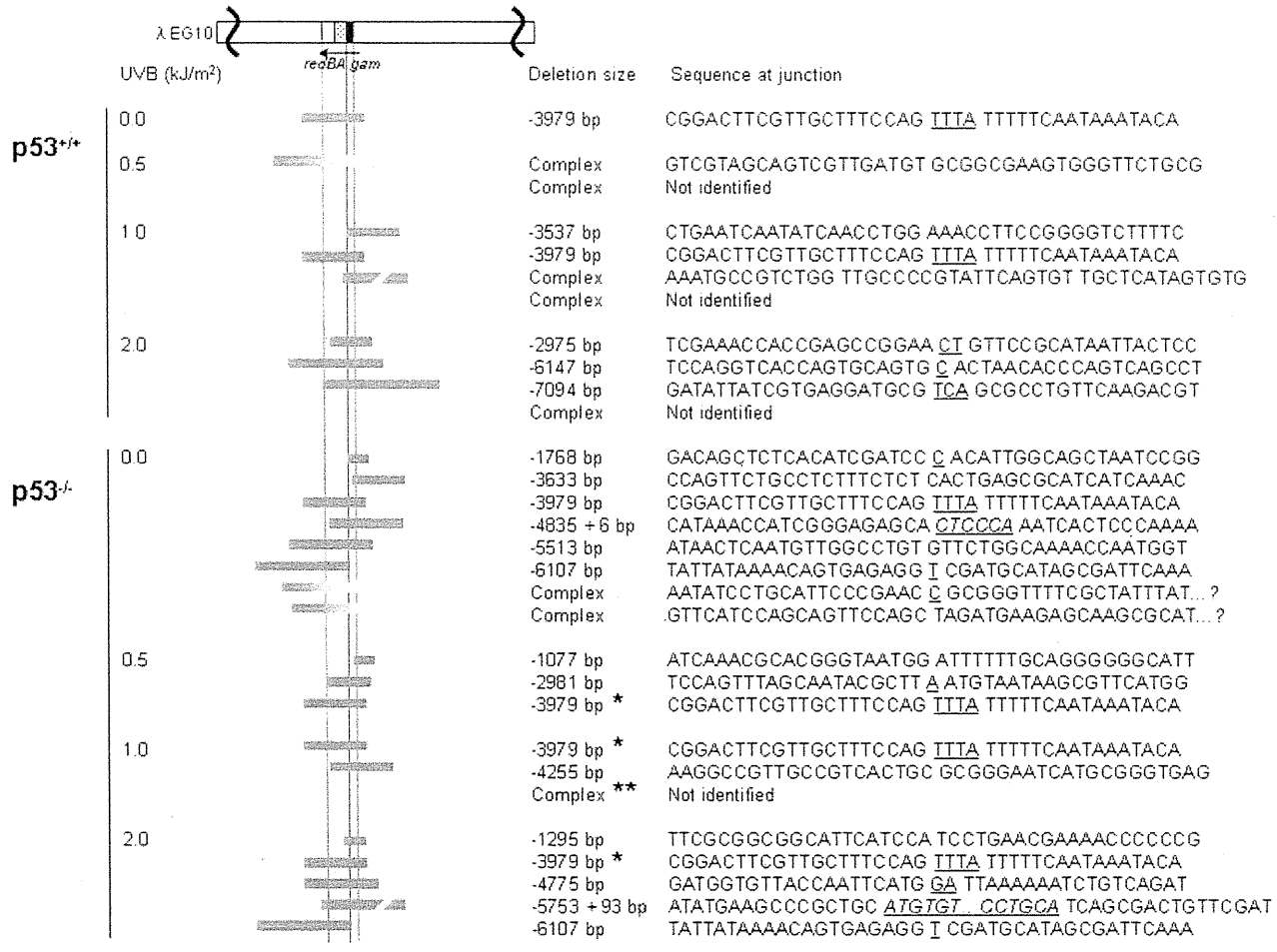

Fig. 3. Molecular nature of large deletions recovered from the epidermis of UVB-irradiated $p53^{+/+}$ and $p53^{-/-}$ *gpt* delta mice. A partial genetic map of the lambda EG10 transgene including the *gam* and *redBA* target region of Spi$^-$ selection is shown in the upper part. Horizontal gray bars represent the deleted regions of mutants. Junctions are indicated as spaces between left and right sequences. Short homologous sequences in the junctions of the mutants are underlined. Underlined, italicized sequences are inserted sequences. *The identical independent mutant was recovered multiple times from the same group: the -3979 bp deletion was recovered from three of four mice for each group (0.5, 1.0, or 2.0 kJ/m^2) of UVB-irradiated $p53^{-/-}$ mice. The complex types were recovered from four $p53^{-/-}$ mice irradiated with 1.0 kJ/m^2 UVB.

I and II). The most frequent point mutations in the epidermis of UVB-irradiated mice were G:C to A:T transitions induced at dipyrimidine sites, such as 5′-TC-3′ and 5′-CC-3′, which were 86–95% and 83–95% of total G:C to A:T transitions in UVB-irradiated $p53^{+/+}$ and $p53^{-/-}$ mice, respectively. From studies on UVB-irradiated *E. coli*, mammalian cells, and the *p53* gene in nonmelanoma skin cancer, it is known that UVB irradiation generates cyclobutane pyrimidine dimers (CPD) and pyrimidime(6-4)pyrimidome photoproducts (6-4PP) at dipyrimidine sites and induces G:C to A:T base substitutions [Miller, 1985; Hauser et al., 1986; Hsia et al., 1989; Brash et al., 1991; Ziegler et al., 1993; Daya-Grosjean et al., 1995]. The spectra of UVB-induced mutations in the epidermis of Muta^{TM} mice were reported to be dominated by G:C to A:T transitions at dipyrimidine sites in the *lacZ* transgene [Ikehata et al., 2003]. The results in this study and previous reports suggest that UVB-induced photoproducts cause characteristic mutations at similar efficiencies in the epidermis of both $p53^{+/+}$ and $p53^{-/-}$ mice.

Interestingly, there were no increases in *gpt* MFs at UVB doses above 0.5 kJ/m^2 in both $p53^{+/+}$ and $p53^{-/-}$ mice (Fig. 1). These results are consistent with the previous observation that the *gpt* MF was increased about nine times by UVB irradiation at 0.3 kJ/m^2, but did not significantly increase more at doses of 0.5–2.0 kJ/m^2 in wild-type *gpt* delta mice [Horiguchi et al., 1999]. These results suggest that *gpt* MFs in the epidermis are saturated at these doses. Ikehata also reported that UVB induction of mutations was suppressed in acute high-dose exposure to the epidermis using Muta^{TM} mice [Ikehata and Ono, 2002]. The suppression occurred even in the absence of p53; therefore, it was not due to p53-dependent antimutagenic effects such as p53-dependent apoptosis. A higher efficiency of DNA repair might be induced at higher UVB doses, or highly

damaged cells might be selectively killed during inflammation induced by UVB irradiation [Ikehata and Ono, 2002]. Whatever the mechanisms are, our results (shown in Fig. 1) raise the possibility that factors other than *p53* contribute to genome stability in the murine epidermis.

UV-induced mutagenesis is induced by translesion DNA synthesis (TLS) that proceeds across UVB-induced photoproducts such as CPD or 6-4PP [Friedberg et al., 2006]. Specialized DNA polymerases involved in lesion bypass have been identified. These polymerases insert incorrect bases such as dGMP opposite the 3′C of CT sites at a relatively high frequency, thereby generating incorrect nascent DNA sequences during DNA synthesis [Prakash et al., 2005]. This process may rescue stalled DNA synthesis at the lesion and contribute to the completion of whole chromosome replication, but it may induce point mutations as byproducts. DNA polymerase iota, kappa, and zeta may be involved in the error-prone TLS across UV-induced photoproducts [Gueranger et al., 2008; Ziv et al., 2009]. These results shown in Figure 1 suggest that p53 may not be involved in the error-prone TLS across UVB-induced lesions. Although the relationship between p53 and TLS by specialized DNA polymerases has not been thoroughly examined, one report suggests that the mutations on plasmids carrying a benzo[*a*]pyrene–induced guanine adduct are suppressed by the presence of p53 in mouse embryonic fibroblasts [Avkin et al., 2004]. In the experiments, the mutation frequencies on the plasmids were higher in cells derived from $p53^{-/-}$ mice than in cells from $p53^{+/+}$ mice. Therefore, it was concluded, that p53 suppressed the error-prone nature of specialized DNA polymerases during the bypass processes. However, our results do not support this conclusion, because the MF and UVB-induced mutation spectra were similar between $p53^{-/-}$ and $p53^{+/+}$ mice. The apparent discrepancy may be due to different experimental conditions, for example, DNA lesions, cell types, and detection methods for mutations. Another possibility may be that higher induction of the *gpt* mutations in $p53^{-/-}$ mice could not be observed because the MFs were already saturated in both $p53^{+/+}$ and $p53^{-/-}$ mice with 0.5 kJ/m^2 irradiation. The effect of p53 may be masked, due to a p53-independent saturation of *gpt* MFs in this study. Further investigation is needed to examine the relationship between p53 and error rates of TLS by multiple specialized DNA polymerases.

In contrast to the *gpt* mutations, where no substantial differences were observed between $p53^{+/+}$ and $p53^{-/-}$ mice, Spi$^-$ MF in unirradiated $p53^{-/-}$ mice was 2.5 times higher than that in $p53^{+/+}$ counterparts, although there is no statistical significance because of the small number of *n* (Table III). Focusing on the specific mutation frequency, in unirradiated $p53^{-/-}$ mice, especially the specific mutation frequencies of large deletions and complex-type rearrangements were significantly higher than those of the large deletions in the $p53^{+/+}$ counterparts (1.58×10^{-6} vs. 0.17×10^{-6}, $P = 0.04$, Dunnet test) (Fig. 2). These deletion and complex-type rearrangements are thought to be induced by nonhomologous end-joining during repair of DSB in DNA [Nohmi and Masumura, 2005]. The higher spontaneous mutation frequencies of large deletions and complex-type rearrangements in $p53^{-/-}$ mice suggests that the antigenotoxic effects of *p53* may be specialized to suppress the mutagenic end-joining process to seal DSB in DNA. This is consistent with previous reports that chromosome alterations, including chromosome loss/duplication and interstitial deletion, are more frequently observed in $p53^{-/-}$ mice compared with $p53^{+/+}$ mice [Shao et al., 2000]. Because of the antimutagenic effects, we expected that the specific Spi$^-$ mutation frequencies for large deletions and complex types would be significantly increased by UVB irradiation in $p53^{-/-}$ mice compared with $p53^{+/+}$ mice. However, the specific mutation frequencies did not increase more than the spontaneous level even after UVB irradiation at doses of 0.5, 1.0, or 2.0 kJ/m^2 in $p53^{-/-}$ mice (Fig. 2). The results suggest the p53-independent antimutagenic mechanisms that suppress *gpt* mutations (discussed earlier) may also act on cells that have DSB in DNA. Currently, the mechanisms are not known but may be related to inflammation in the skin induced by UVB irradiation [Ikehata and Ono, 2002]. Alternatively, p53 may be positively involved in induction of deletions and complex-type mutations induced by UVB; therefore, there was no increase in the Spi$^-$ mutation frequency in UVB-irradiated $p53^{-/-}$ mice. It is reported that DSB in DNA are induced during the repair of UV photoproducts [Bradley and Taylor, 1981]. It is known that p53 is involved in nucleotide excision repair (NER) [Ford and Hanawalt, 1995, 1997; Smith et al., 2000] and p53 regulates the expression of several NER genes including *XPC* and *DDB2* [Hwang et al., 1999; Adimoolam and Ford, 2002]. Thus, p53 may be involved in the induction of large deletions by regulating the repair of UVB photoproducts. If this is the case, Spi$^-$ large deletions will not be induced in $p53^{-/-}$ mice after UVB irradiation. However, it is possible that the small number of mice and the relatively high background mutation frequency may obscure an effect of UVB in $p53^{-/-}$ mice, because increase in the specific Spi$^-$ mutation frequency caused by UVB is very small even in $p53^{+/+}$ mice. To answer this issue, larger number of mice and improved experimental design may be needed.

The MFs of Spi$^-$ deletions in $p53^{+/-}$ mice increased twofold to fourfold when compared with the control level at UVB doses of 0.5, 1.0, or 2.0 kJ/m^2 (Table III). In a previous study, we observed suppression of UVB-induced large deletions at UVB doses of 1.0, 1.5, or 2.0 kJ/m^2; therefore, the dose–response curve was a bell-shaped one [Horiguchi et al., 2001]. In this study, we did not observe such strong suppression of the Spi$^-$ MF at UVB doses of 1.0 and 2.0 kJ/m^2 (Fig. 2). The apparent discrepancy between the previous and current studies might be due to the different irradia-

tion conditions such as dose rates and UVB sources. The dose rate used in this study was 0.3 kJ/m^2/min [5 J/m^2/s], which is lower than that used in the previous study [17 J/m^2/s]; although, total doses were similar. A handheld UV lamp in a cabinet was used in this study instead of the straight-tube fluorescent lights used in the previous study. The different wavelength distribution of UV from different lamps could also affect the dose responses. When we focus on the larger deletions (greater than 1 kb) and complex types, the specific Spi$^-$ MFs of *p53*$^{+/+}$ mice significantly increased, up to 5.5-fold higher than the control level at 2.0 kJ/m^2 (0.93×10^{-6} vs. 0.17×10^{-6}) (Fig. 2). However, the specific MF of large deletions and complex types was increased 17-fold in the previous study [Horiguchi et al., 2001]. The lower dose rate used in this study may have caused relatively weaker induction of larger deletions. Dose rate might be an important factor for UVB-induced large deletions driven by DSB and end-joining.

Thirty-nine Spi$^-$ large deletions (greater than 1 kb), recovered from both *p53*$^{+/+}$ and *p53*$^{-/-}$ mice, were sequenced and are shown in Figure 3. The majority of those deletions have short homologous sequences of 1–4 bp at the junction in both *p53*$^{+/+}$ and *p53*$^{-/-}$ mice. The largest deletion size identified was −7,094 bp. The Spi$^-$ mutation assays can detect a simultaneous inactivation of both the *gam* and *red* genes, which is usually induced by deletions. Because of the size limitation for lambda in vitro packaging reactions (there must be two cos sites separated by 38–51 kb of DNA), deletions up to 10 kb are detectable as Spi$^-$ mutations [Nohmi and Masumura, 2004, 2005]. Interestingly, an identical −3,979 bp deletion having a 4 bp (5-TTTA-3′) microhomology at the junction was repeatedly observed in both *p53*$^{+/+}$ and *p53*$^{-/-}$ mice. This deletion is not UV-dependent because the same deletion was also independently recovered from the unirradiated epidermis. In the previous study, the same deletion was also observed multiple times in both UVB-irradiated and UVB-unirradiated epidermis (six independent mutations were recovered from 12 mice) [Horiguchi et al., 2001]. In contrast, this deletion was not observed in other tissues, with the exception of 1 identified from the liver out of more than 400 independent Spi$^-$ mutants previously sequenced [Yatagai et al., 2002; Nohmi and Masumura, 2004]. This −3,979 bp Spi$^-$ deletion may be a hot spot mutation in the epidermis of the mouse. In human skin, a −3,895 bp deletion in mitochondrial DNA was proposed to be a marker for sunlight exposure [Krishnan et al., 2004]. It has a 12-bp microhomology at the junction (5′-CCATACCCCGAA-3′). The relationship between the −3,979 bp deletion in the chromosome DNA of the murine epidermis and the −3,895 bp deletion in the mitochondria DNA in human skin is currently unknown.

Several p53-deficient mouse strains were previously developed to investigate the function of p53 in mutagenesis by in vivo mutation detection systems using *lacZ*, *lacI*, *aprt*, etc. [Morris, 2002]. Those mouse models have a common phenotype, a propensity to develop thymic lymphoma. However, the effect of p53 on spontaneous and mutagen-induced mutations has not been thoroughly investigated. In this study, we investigated the role of p53 in spontaneous and UV-induced mutations, including both point mutations and deletions, in the mouse epidermis. The results showed that p53 may suppress spontaneous deletions. This implies that once p53 is inactivated, the mutated cells will display high levels of genome instability, even without additional exposure to sunlight or other environmental mutagens. To better understand p53 functions in mutagenesis in vivo, it is important to further investigate how p53 is involved in several cellular functions such as DNA damage-response and repair pathways.

REFERENCES

Adams WT, Skopek TR. 1987. Statistical test for the comparison of samples from mutational spectra. J Mol Biol 194:391–396.

Adimoolam S, Ford JM. 2002. p53 and DNA damage-inducible expression of the xeroderma pigmentosum group C gene. Proc Natl Acad Sci USA 99:12985–12990.

Aubrecht J, Secretan MB, Bishop AJ, Schiestl RH. 1999. Involvement of p53 in X-ray induced intrachromosomal recombination in mice. Carcinogenesis 20:2229–2236.

Avkin S, Goldsmith M, Velasco-Miguel S, Geacintov N, Friedberg EC, Livneh Z. 2004. Quantitative analysis of translesion DNA synthesis across a benzo[*a*]pyrene–guanine adduct in mammalian cells: The role of DNA polymerase kappa. J Biol Chem 279:53298–53305.

Bradley MO, Taylor VI. 1981. DNA double-strand breaks induced in normal human cells during the repair of ultraviolet light damage. Proc Natl Acad Sci USA 78:3619–3623.

Brash DE, Rudolph JA, Simon JA, Lin A, McKenna GJ, Baden HP, Halperin AJ, Ponten J. 1991. A role for sunlight in skin cancer: UV-induced p53 mutations in squamous cell carcinoma. Proc Natl Acad Sci USA 88:10124–10128.

Buettner VL, Hill KA, Nishino H, Schaid DJ, Frisk CS, Sommer SS. 1996. Increased mutation frequency and altered spectrum in one of four thymic lymphomas derived from tumor prone *p53*/Big Blue double transgenic mice. Oncogene 13:2407–2413.

Cariello NF, Piegorsch WW, Adams WT, Skopek TR. 1994. Computer program for the analysis of mutational spectra: Application to *p53* mutations. Carcinogenesis 15:2281–2285.

Daya-Grosjean L, Dumaz N, Sarasin A. 1995. The specificity of *p53* mutation spectra in sunlight induced human cancers. J Photochem Photobiol B 28:115–124.

Donehower LA, Harvey M, Slagle BL, McArthur MJ, Montgomery CA Jr., Butel JS, Bradley A. 1992. Mice deficient for p53 are developmentally normal but susceptible to spontaneous tumours. Nature 356:215–221.

Ford JM, Hanawalt PC. 1995. Li–Fraumeni syndrome fibroblasts homozygous for *p53* mutations are deficient in global DNA repair but exhibit normal transcription-coupled repair and enhanced UV resistance. Proc Natl Acad Sci USA 92:8876–8880.

Ford JM, Hanawalt PC. 1997. Expression of wild-type p53 is required for efficient global genomic nucleotide excision repair in UV-irradiated human fibroblasts. J Biol Chem 272:28073–28080.

Friedberg EC, Walker GC, Siede W, Wood RD, Schultz RA, Ellenberger T. 2006. DNA Repair and Mutagenesis. 2nd ed. Washington, DC: ASM press. 1118 p.

Gueranger Q, Stary A, Aoufouchi S, Faili A, Sarasin A, Reynaud CA, Weill JC. 2008. Role of DNA polymerases eta, iota and zeta in UV resistance and UV-induced mutagenesis in a human cell line. DNA Repair (Amst) 7:1551–1562.

Hauser J, Seidman MM, Sidur K, Dixon K. 1986. Sequence specificity of point mutations induced during passage of a UV-irradiated shuttle vector plasmid in monkey cells. Mol Cell Biol 6:277–285.

Horiguchi M, Masumura K, Ikehata H, Ono T, Kanke Y, Sofuni T, Nohmi T. 1999. UVB-induced *gpt* mutations in the skin of *gpt* delta transgenic mice. Environ Mol Mutagen 34:72–79.

Horiguchi M, Masumura K, Ikehata H, Ono T, Kanke Y, Nohmi T. 2001. Molecular nature of ultraviolet B light-induced deletions in the murine epidermis. Cancer Res 61:3913–3918.

Hsia HC, Lebkowski JS, Leong PM, Calos MP, Miller JH. 1989. Comparison of ultraviolet irradiation-induced mutagenesis of the *lacI* gene in *Escherichia coli* and in human 293 cells. J Mol Biol 205:103–113.

Hwang BJ, Ford JM, Hanawalt PC, Chu G. 1999. Expression of the p48 xeroderma pigmentosum gene is p53-dependent and is involved in global genomic repair. Proc Natl Acad Sci USA 96:424–428.

Ikehata H, Ono T. 2002. Mutation induction with UVB in mouse skin epidermis is suppressed in acute high-dose exposure. Mutat Res 508:41–47.

Ikehata H, Aiba S, Ozawa H, Ono T. 2001. Thermolysin improves mutation analysis in skin epidermis from ultraviolet light-irradiated Muta mouse. Environ Mol Mutagen 38:55–58.

Ikehata H, Masuda T, Sakata H, Ono T. 2003. Analysis of mutation spectra in UVB-exposed mouse skin epidermis and dermis: Frequent occurrence of C→T transition at methylated CpG-associated dipyrimidine sites. Environ Mol Mutagen 41:280–292.

Ikehata H, Nakamura S, Asamura T, Ono T. 2004. Mutation spectrum in sunlight-exposed mouse skin epidermis: Small but appreciable contribution of oxidative stress-mediated mutagenesis. Mutat Res 556:11–24.

Jacks T, Remington L, Williams BO, Schmitt EM, Halachmi S, Bronson RT, Weinberg RA. 1994. Tumor spectrum analysis in p53-mutant mice. Curr Biol 4:1–7.

Krishnan KJ, Harbottle A, Birch-Machin MA. 2004. The use of a 3895 bp mitochondrial DNA deletion as a marker for sunlight exposure in human skin. J Invest Dermatol 123:1020–1024.

Lambert IB, Singer TM, Boucher SE, Douglas GR. 2005. Detailed review of transgenic rodent mutation assays. Mutat Res 590:1–280.

Miller JH. 1985. Mutagenic specificity of ultraviolet light. J Mol Biol 182:45–65.

Morris SM. 2002. A role for p53 in the frequency and mechanism of mutation. Mutat Res 511:45–62.

Nishino H, Knoll A, Buettner VL, Frisk CS, Maruta Y, Haavik J, Sommer SS. 1995. p53 wild-type and p53 nullizygous Big Blue transgenic mice have similar frequencies and patterns of observed mutation in liver, spleen and brain. Oncogene 11:263–270.

Nohmi T. 2007. Novel DNA polymerases and novel genotoxicity assays. Genes Environ 29:75–88.

Nohmi T, Masumura K. 2004. *Gpt* delta transgenic mouse: A novel approach for molecular dissection of deletion mutations in vivo. Adv Biophys 38:97–121.

Nohmi T, Masumura K. 2005. Molecular nature of intrachromosomal deletions and base substitutions induced by environmental mutagens. Environ Mol Mutagen 45:150–161.

Nohmi T, Katoh M, Suzuki H, Matsui M, Yamada M, Watanabe M, Suzuki M, Horiya N, Ueda O, Shibuya T, Ikeda H, Sofuni T. 1996. A new transgenic mouse mutagenesis test system using Spi and 6-thioguanine selections. Environ Mol Mutagen 28:465–470.

Nohmi T, Suzuki T, Masumura K. 2000. Recent advances in the protocols of transgenic mouse mutation assays. Mutat Res 455:191–215.

Prakash S, Johnson RE, Prakash L. 2005. Eukaryotic translesion synthesis DNA polymerases: Specificity of structure and function. Annu Rev Biochem 74:317–353.

Purdie CA, Harrison DJ, Peter A, Dobbie L, White S, Howie SE, Salter DM, Bird CC, Wyllie AH, Hooper ML. 1994. Tumour incidence, spectrum and ploidy in mice with a large deletion in the *p53* gene. Oncogene 9:603–609.

Sands AT, Suraokar MB, Sanchez A, Marth JE, Donehower LA, Bradley A. 1995. p53 deficiency does not affect the accumulation of point mutations in a transgene target. Proc Natl Acad Sci USA 92:8517–8521.

Shao C, Deng L, Henegariu O, Liang L, Stambrook PJ, Tischfield JA. 2000. Chromosome instability contributes to loss of heterozygosity in mice lacking p53. Proc Natl Acad Sci USA 97:7405–7410.

Shibata A, Masutani M, Nozaki T, Kamada N, Fujihara H, Masumura K, Nakagama H, Sugimura T, Kobayashi S, Suzuki H, Nohmi T. 2003. Improvement of the Spi⁻ assay for mutations in *gpt* delta mice by including magnesium ions during plaque formation. Environ Mol Mutagen 41:370–372.

Smith ML, Ford JM, Hollander MC, Bortnick RA, Amundson SA, Seo YR, Deng CX, Hanawalt PC, Fornace AJ Jr. 2000. p53-mediated DNA repair responses to UV radiation: Studies of mouse cells lacking *p53*, *p21*, and/or *gadd45* genes. Mol Cell Biol 20:3705–3714.

Tsukada T, Tomooka Y, Takai S, Ueda Y, Nishikawa S, Yagi T, Tokunaga T, Takeda N, Suda Y, Abe S. 1993. Enhanced proliferative potential in culture of cells from p53-deficient mice. Oncogene 8:3313–3322.

Yatagai F, Kurobe T, Nohmi T, Masumura K, Tsukada T, Yamaguchi H, Kasai-Eguchi K, Fukunishi N. 2002. Heavy-ion-induced mutations in the gpt delta transgenic mouse: Effect of *p53* gene knockout. Environ Mol Mutagen 40:216–225.

Ziegler A, Leffell DJ, Kunala S, Sharma HW, Gailani M, Simon JA, Halperin AJ, Baden HP, Shapiro PE, Bale AE. 1993. Mutation hotspots due to sunlight in the *p53* gene of nonmelanoma skin cancers. Proc Natl Acad Sci USA 90:4216–4220.

Ziv O, Geacintov N, Nakajima S, Yasui A, Livneh Z. 2009. DNA polymerase zeta cooperates with polymerases kappa and iota in translesion DNA synthesis across pyrimidine photodimers in cells from XPV patients. Proc Natl Acad Sci USA 106:11552–11557.

Accepted by—
J. Fuscoe

Mutagenic potency of *Helicobacter pylori* in the gastric mucosa of mice is determined by sex and duration of infection

Alexander Sheh[a], Chung Wei Lee[a,b], Kenichi Masumura[c], Barry H. Rickman[b], Takehiko Nohmi[c], Gerald N. Wogan[a,1], James G. Fox[a,b,2], and David B. Schauer[a,b,2]

[a]Department of Biological Engineering, Massachusetts Institute of Technology, Cambridge, MA 02139; [b]Division of Comparative Medicine, Massachusetts Institute of Technology, Cambridge, MA 02139; and [c]Division of Genetics and Mutagenesis, National Institute of Health Sciences, Tokyo 158-8501, Japan

Contributed by Gerald N. Wogan, July 19, 2010 (sent for review April 27, 2010)

Helicobacter pylori **is a human carcinogen, but the mechanisms evoked in carcinogenesis during this chronic inflammatory disease remain incompletely characterized. We determined whether chronic *H. pylori* infection induced mutations in the gastric mucosa of male and female *gpt* delta C57BL/6 mice infected for 6 or 12 mo. Point mutations were increased in females infected for 12 mo. The mutation frequency in this group was 1.6-fold higher than in uninfected mice of both sexes ($P < 0.05$). A:T-to-G:C transitions and G:C-to-T:A transversions were 3.8 and 2.0 times, respectively, more frequent in this group than in controls. Both mutations are consistent with DNA damage induced by oxidative stress. No increase in the frequency of deletions was observed. Females had more severe gastric lesions than males at 6 mo postinfection (MPI; $P < 0.05$), but this difference was absent at 12 MPI. In all mice, infection significantly increased expression of *IFNγ*, *IL-17*, *TNFα*, and *iNOS* at 6 and 12 mo, as well as *H. pylori*–specific IgG1 levels at 12 MPI ($P < 0.05$) and IgG2c levels at 6 and 12 MPI ($P < 0.01$ and $P < 0.001$). At 12 MPI, IgG2c levels in infected females were higher than at 6 MPI ($P < 0.05$) and also than those in infected males at 12 MPI ($P < 0.05$). Intensity of responses was mediated by sex and duration of infection. Lower *H. pylori* colonization indicated a more robust host response in females than in males. Earlier onset of severe gastric lesions and proinflammatory, Th1-biased responses in female C57BL/6 mice may have promoted mutagenesis by exposing the stomach to prolonged oxidative stress.**

gpt delta mouse | *Helicobacter* | inflammation | mutagenesis | sexual dimorphism

Acting through multiple, complex mechanisms that are incompletely understood, chronic inflammation is a significant risk factor for several major human malignancies, including stomach cancer. Chronic inflammation induced by *Helicobacter pylori* infection increases lifetime risk of developing gastritis, duodenal and gastric ulcers, mucosa-associated lymphoid tissue lymphoma, mucosal atrophy, and gastric carcinoma (1, 2). Indeed, *H. pylori* has been classified by International Agency for Research on Cancer as a group I human carcinogen on the basis of its impact on gastric cancer incidence, the second most frequent cause of cancer-related death worldwide (3). Among postulated mechanisms through which infection may contribute to increased cancer risk are overproduction of reactive oxygen and nitrogen species (RONS) by inflammatory cells, and the consequent induction of mutations critical for tumor initiation in cells of inflamed tissues (4). The inflammatory response to infection results in increased production of RONS, including superoxide ($O_2^{-}\cdot$), hydrogen peroxide (H_2O_2), nitric oxide (NO), peroxynitrite (ONO_2^-), and nitrous anhydride (N_2O_3), in vitro (5, 6) and in vivo (7–9). *H. pylori* can also directly activate RONS-producing enzymes, such as inducible NO synthase (iNOS) and spermine oxidase, in gastric epithelial cells, causing DNA damage and apoptosis (5, 6). Chronic inflammatory states increase levels of DNA adducts, such as etheno adducts, 8-oxoG, and other mutagenic precursors, in vitro and in vivo (10–12), but tend not to alter the frequency of deletions (13). RONS also can damage DNA indirectly by creating adduct-forming electrophiles via lipid peroxidation (14, 15). RONS have been shown to induce mutations in *H. pylori* by inducing a hypermutation state in the bacteria (16).

A widely used experimental model is the *H. pylori* SS1-infected C57BL/6 mouse, which is susceptible to chronic infection and develops robust gastritis and premalignant lesions similar to those occurring in humans (17, 18). To date, limited investigation has focused on genetic damage associated with infection in these animals, but available data are still incomplete. Enhanced DNA fragmentation was observed in gastric cells of infected mice (19), in which dsDNA breaks were also detected by TUNEL assay (20, 21). Mutagenicity in reporter genes recovered from gastric DNA of male and female Big Blue transgenic mice 6 mo after infection with *H. pylori* or *Helicobacter felis* has also been reported (22). In *H. pylori*-infected male mice, point mutation frequency was increased at 6 mo post infection (MPI), but decreased to control levels by 12 MPI, suggesting that the animals may have adapted to infection (22). Female mice infected with *H. felis* also had an increased frequency of point mutations at 7 MPI, compared with uninfected controls (23). Mutagenesis resulting from infection has also been associated with p53 status. Mutations were found in the *lacI* reporter genes of a small number of *H. felis*-infected female TSG-p53/Big Blue mice harboring either one ($p53^{+/-}$) or two ($p53^{+/+}$) WT p53 alleles (23). A 2-fold increase in mutations was found in DNA from the gastric mucosa of infected $p53^{+/+}$ mice, and also in uninfected $p53^{+/-}$ mice; the mutation frequency in infected $p53^{+/-}$ mice was further increased by approximately threefold. The intensity of inflammation was estimated to be significantly higher in infected $p53^{+/-}$ mice than in infected $p53^{+/+}$ animals, and gastric epithelial proliferation was similarly increased with infection in both latter treatment groups. By contrast, in another study, infection of Big Blue transgenic mice (sex not specified) with the SS1 strain of *H. pylori* for 3.5 mo resulted in no significant increase in gastric mutations over uninfected controls (13).

We used the *gpt* delta mouse to measure the accumulation of gastric mutations associated with *H. pylori* SS1 infection in male and female animals at 6 and 12 MPI. This experimental system comprises λ-EG10–based transgenic C57BL/6 mice harboring tandem arrays of 80 copies of the bacterial *gpt* gene at a single site on chromosome 17. The model was specifically designed to facilitate the in vivo detection of point mutations by 6-thioguanine

Author contributions: A.S., C.W.L., J.G.F., and D.B.S. designed research; A.S., C.W.L., and B.H.R. performed research; K.M. and T.N. contributed new reagents/analytic tools; A.S., B.H.R., G.N.W., J.G.F., and D.B.S. analyzed data; and A.S., G.N.W., and J.G.F. wrote the paper.

The authors declare no conflict of interest.

[1]To whom correspondence should be addressed. E-mail: wogan@mit.edu.

[2]J.G.F. and D.B.S. contributed equally to this work.

This article contains supporting information online at www.pnas.org/lookup/suppl/doi:10.1073/pnas.1009017107/-/DCSupplemental.

MICROBIOLOGY

(6-TG) selection, and deletions up to 10 kb in length by selection based on sensitivity to P2 interference (Spi^-) (24). When phage DNA rescued from mouse tissues is introduced into appropriate *Escherichia coli* strains, both point mutations and large deletions can be efficiently detected (24). We also characterized histopathologic changes, expression of inflammatory cytokines, and expression of iNOS in gastric mucosa 6 and 12 mo after initial infection. In addition, we compared responses of male and female mice to assess the influence of sex. We found that *H. pylori* infection induced significant increases in the frequency of point mutations in the gastric mucosa of female, but not male, *gpt* delta mice. The accumulation of point mutations was therefore sex-dependent and was mediated by the duration of infection and the severity of disease.

Results and Discussion

Pathology, Cytokine and iNOS Expression, and Serologic Responses to *H. pylori* Infection and *H. pylori* Levels. Inflammatory histopathologic changes resulting from *H. pylori* infection were evaluated (Fig. S1) and gastric histological activity index (GHAI) scores calculated, with the following results. Scores were significantly increased in infected animals of both sexes at 6 and 12 MPI (female, $P < 0.001$ and $P < 0.01$, respectively; and male, $P < 0.05$ and $P < 0.001$, respectively; Fig. 1). Regarding specific types of lesions represented in the GHAI, infected females experienced higher levels of hyperplasia ($P < 0.05$), epithelial defects ($P < 0.001$), and dysplasia ($P < 0.05$) compared with infected males at 6 MPI, and thus had correspondingly higher ($P < 0.05$) GHAI scores at this time point. At 6 MPI, infected animals of both sexes displayed mild to moderate inflammation, comprised chiefly of submucosal and mucosal infiltrates of mononuclear and granulocytic cells. In addition, in infected males, mucous metaplasia, intestinal metaplasia, oxyntic gland atrophy, and hyalinosis were all significantly elevated compared with controls (all $P < 0.01$; intestinal metaplasia, $P < 0.001$); no significant increases occurred in foveolar hyperplasia, epithelial defects, or dysplasia. In infected females, inflammation ($P < 0.05$), epithelial defects ($P < 0.001$), mucous metaplasia ($P < 0.01$), hyalinosis ($P < 0.001$), as well as premalignant lesions of oxyntic gland atrophy ($P < 0.001$), intestinal metaplasia ($P < 0.05$), and dysplasia ($P < 0.05$) were significantly elevated compared with uninfected controls. At 12 MPI, there were no differences in gastric lesion severity between infected males and females; both groups had similar mucosal changes. Infected male mice at 12 MPI displayed significantly increased epithelial defects but decreased intestinal metaplasia than infected males at 6 MPI ($P < 0.01$ and $P < 0.001$).

H. pylori infection significantly increased transcription profiles at 6 and 12 MPI as follows (details in Fig. S2): *IFNγ* (males, $P < 0.001$; females, $P < 0.01$ at 6 and 12 MPI); *TNF-α* (males, $P < 0.01$ at 6 and 12 MPI; females, $P < 0.01$ and $P < 0.05$); *IL-17* (males, $P < 0.05$ and $P < 0.001$; females, $P < 0.05$ and $P < 0.01$). *iNOS* expression was increased in male and female mice at 6 and 12 MPI (males, $P < 0.05$ and $P < 0.01$; females, $P < 0.01$ and $P < 0.001$) compared with controls at 12 mo. *IL-10* expression was not significantly affected by infection in animals of either sex ($P > 0.05$).

H. pylori infection also resulted in a Th1-predominant IgG2c response in infected mice as previously reported (25, 26) (Fig. 2). *H. pylori*-specific IgG2c levels were higher in infected than in uninfected animals at 6 and 12 MPI ($P < 0.01$ and $P < 0.001$, respectively). At 12 MPI, infected females had significantly higher

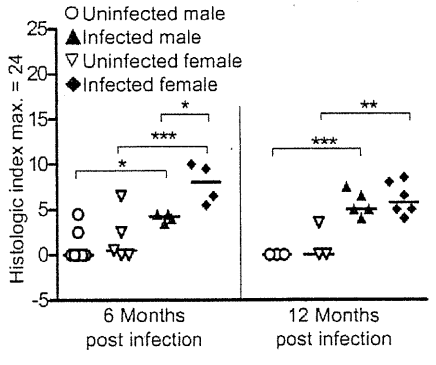

Fig. 1. *H. pylori* infection elicits more gastric pathologic processes in female mice at 6 mo. *H. pylori* infection increased the GHAI in both male and female C57BL/6 mice at 6 and 12 mo. At 6 mo of infection, infected females had significantly more pathologic processes than infected males. Uninfected males (○; 6 MPI, $n = 7$; 12 MPI, $n = 3$), uninfected females (▽; 6 MPI, $n = 5$; 12 MPI, $n = 3$), infected males (▼; 6 MPI, $n = 4$; 12 MPI, $n = 5$) and infected females (◆; 6 MPI, $n = 4$; 12 MPI, $n = 6$). Bar represents the mean. $^*P < 0.05$, $^{**}P < 0.01$, and $^{***}P < 0.001$.

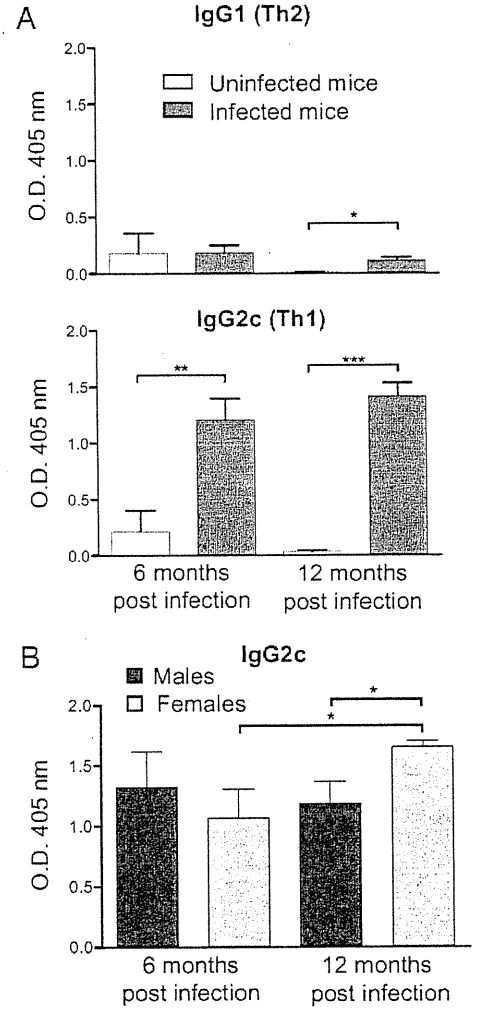

Fig. 2. The effect of *H. pylori* infection on *H. pylori*–specific IgG1 and IgG2c. Serum levels of IgG were measured by ELISA in uninfected and *H. pylori*–infected mice. (*A*) *H. pylori*–infected mice (gray bars; 6 MPI, $n = 9$; 12 MPI, $n = 12$) developed a greater IgG1 response after 12 mo of infection compared with uninfected mice (white bars; 6 MPI, $n = 6$; 12 MPI, $n = 6$; $P < 0.05$). *H. pylori*–infected mice developed a greater IgG2 response after 6 and 12 mo of infection ($P < 0.01$ and $P < 0.001$, respectively). (*B*) At 12 mo, infected female mice (light gray bars; 6 MPI, $n = 4$; 12 MPI, $n = 6$) had substantially increased IgG2c compared with infected males (dark gray bars; 6 MPI, $n = 5$; 12 MPI, $n = 6$) at 12 mo and infected females at 6 mo ($P < 0.05$, both). Data are mean (SE) of mice in different treatment groups. $^*P < 0.05$, $^{**}P < 0.01$, and $^{***}P < 0.001$.

IgG2c levels than infected males ($P < 0.05$). Duration of infection also increased IgG2c levels in infected females, with higher levels noted at 12 versus 6 MPI ($P < 0.05$). *H. pylori*-specific IgG1 (Th2) levels were higher in infected than in uninfected animals at 12 MPI ($P < 0.05$). Females had higher Th1/Th2 ratios than males: at 6 MPI, 8.58 vs. 4.01; and at 12 MPI, 12.9 vs. 7.51.

We and others have demonstrated that *H. pylori* levels are inversely correlated with the degree of pathology and the immune response as measured by antibody and cytokine production (25, 27). At 6 MPI, *H. pylori* was detectable by quantitative PCR in all infected males, but not in one female. At 12 MPI, there was a salient difference in levels of *H. pylori* colonization between males and females; *H. pylori* was undetectable in four infected females, but undetectable in only one male (Fig. 3).

Frequency and Nature of Mutations. We determined the frequency of *gpt* point mutations in gastric DNA isolated from infected and uninfected mice by selection of mutants based on 6-TG resistance. Recognizing the possible confounding effect of clonal expansion of sibling mutants (i.e., jackpot mutations), we sequenced the *gpt* genes from all 566 recovered mutants. Any mutation found to duplicate another at the same site within an individual sample was excluded from subsequent frequency calculations. After this adjustment, at 12 MPI the *gpt* mutation frequency in infected females ($7.5 \pm 2.0 \times 10^{-6}$; $P < 0.05$) was significantly (1.6-fold) higher than that in all control animals ($4.7 \pm 1.1 \times 10^{-6}$), whereas the frequency in infected males ($6.3 \pm 5.4 \times 10^{-6}$; $P = 0.49$) was not. At 6 MPI, *gpt* mutation frequency in infected animals of either sex (females, $5.6 \pm 2.0 \times 10^{-6}$, $P = 0.72$; males, $7.2 \pm 2.2 \times 10^{-6}$, $P = 0.57$) was not significantly different from that of controls ($6.2 \pm 3.0 \times 10^{-6}$; Fig. 4).

After sequencing and accounting for clonal expansion, 236 from infected and 156 mutants from uninfected mice were used to identify effects of *H. pylori* infection on types of mutations causing loss of *gpt* function, with the results summarized in Table 1 and Table S1. G:C-to-A:T transitions and G:C-to-T:A transversions were the most prevalent types of mutations in both infected and uninfected animals, representing 33% to 50% and 17% to 31%, respectively, of total mutations in various treatment groups; mutant frequencies varied from 2.1 to 3.0×10^{-6} in these transitions and 0.9–1.8×10^{-6} in the transversions. The 1.6-fold higher total mutations observed in infected females compared with age-matched controls at 12 MPI was attributable mainly to two types of mutations: 3.8 times more A:T-to-G:C transitions ($P < 0.05$) and 2.0 times more G:C-to-T:A transversions ($P <$

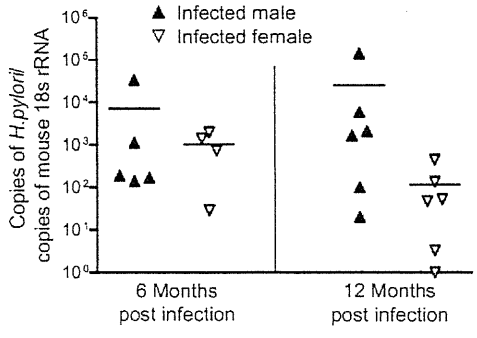

Fig. 3. *H. pylori* levels in the stomach were lower in infected females at 12 MPI. Values represent the number of *H. pylori* organisms per copies of mouse 18s rRNA. At 6 MPI, one infected female mouse was under the threshold of detection (15 copies of *H. pylori*). At 12 MPI, four infected females and one infected male were undetectable. Infected males (▼; 6 MPI, $n = 5$; 12 MPI, $n = 6$) and infected females (▽; 6 MPI, $n = 4$; 12 MPI, $n = 6$). Bar represents the mean.

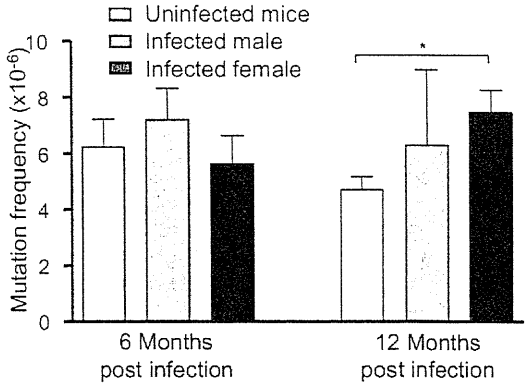

Fig. 4. Twelve-month infection with *H. pylori* increases the frequency of point mutations in female mice. The mutation frequency of point mutations was determined by the *gpt* assay in uninfected mice (white bars; 6 MPI, $n = 13$; 12 MPI, $n = 15$), *H. pylori*-infected males (light gray bars; 6 MPI, $n = 4$; 12 MPI, $n = 5$) and *H. pylori*-infected females (dark gray bars; 6 MPI, $n = 9$; 12 MPI, $n = 11$). Control mice of both sexes were grouped for this analysis. Data are mean (SEM) of mutation frequency of mice in different treatment groups. $^*P < 0.05$.

0.05). These two mutations are consistent with the expected mutational spectrum induced by RONS (28) and have been found elevated in another animal model of chronic inflammation (13). An increase in G:C-to-T:A transversions was also reported in a previous study documenting *H. pylori*-induced mutations (22).

A:T-to-G:C transitions can be formed by deamination of adenine to hypoxanthine or creation of ethenoadenine. Deamination is mediated by N_2O_3, the autoxidation product of NO·, which directly nitrosates primary amines on DNA bases (28, 29). Hypoxanthine resembles guanine and mispairs with cytosine, resulting in the observed mutation. Alternatively, A:T-to-G:C transitions can also be created indirectly by lipid peroxidation by RONS, forming etheno adducts in DNA such as highly mutagenic ethenoadenine (30, 31). G:C-to-T:A transversions have also been associated with increased *iNOS* expression levels, pointing to the involvement of RONS (32). Cells cocultivated with activated macrophages predominantly develop G:C to T:A transversions caused by exposure to NO·, O_2^{-}·, and H_2O_2 (33). G:C-to-T:A transversions are also caused by adducts produced by oxidative stress or lipid peroxidation, such as 8-oxodG, edC, and M1G (34, 35). The presence of 8-oxodG, a major product of oxidative damage to DNA, results in mispairing of guanine with adenine during replication, thus inducing transversions (36). Although 8-oxodG is believed to be the main cause of this mutation, etheno adducts formed by lipid peroxidation may also play a significant role in mutagenesis observed in vivo (37).

Fig. S3 shows the mutation spectrum detected in the *gpt* gene, of which the following features are noteworthy. In both uninfected and infected mice, hotspots occurred at nucleotides C64, G110, G115, and G418; C64, G110, and G115 are CpG sites and are known hotspots in this assay (38, 39). Hotspots occurring in infected mice were located at A8, G116, and G143; A8 and G116 were found predominantly in infected females at both 6 and 12 mo, whereas G143, located at a CpG site, was a hotspot in infected animals of both sexes. Uninfected mice had hotspots at G406, G416, and A419, one of which (G416) occurred mainly in males. Mutations in infected males were concentrated mainly in hotspots common to both uninfected and infected animals, whereas in infected females there was an increase in mutations throughout the *gpt* gene at non-G:C sites. This result suggests that the chemistry of DNA damage in mice with a stronger host response to infection may have differed from that in mice with mild or minimal gastritis.

Table 1. Twelve months of *H. pylori* infection increases the mutation frequency of A:T-to-G:C transitions and G:C-to-T:A transversions in female mice

	6 mo			12 mo		
Effect	Uninfected all (n = 6)	Infected male (n = 4)	Infected female (n = 8)	Uninfected all (n = 14)	Infected male (n = 5)	Infected female (n = 11)
Transition						
G:C to A:T	3.02 (2.07)	2.41 (2.64)	2.74 (1.07)	2.13 (0.87)	2.66 (1.70)	2.69 (0.97)
A:T to G:C	0.27 (0.61)	0.00	0.16 (0.22)	0.23 (0.19)	0.08 (0.16)	0.88 (0.59)*
Transversion						
G:C to T:A	1.30 (1.34)	1.64 (1.29)	0.89 (0.68)	0.85 (0.62)	1.69 (2.43)	1.75 (0.54)*
G:C to C:G	0.29 (0.66)	0.36 (0.71)	0.40 (0.60)	0.19 (0.27)	0.84 (1.25)	0.09 (0.14)
A:T to T:A	0.34 (0.47)	0.00	0.37 (0.37)	0.31 (0.41)	0.00	0.53 (0.89)
A:T to C:G	0.00	0.36 (0.71)	0.18 (0.22)	0.05 (0.12)	0.00	0.25 (0.46)
Deletion						
1-bp deletion	0.84 (0.94)	2.44 (3.99)	0.66 (0.43)	0.53 (0.35)	0.67 (0.54)	0.88 (0.73)
≥2-bp deletion	0.04 (0.12)	0.00	0.44 (0.57)	0.22 (0.20)	0.18 (0.36)	0.22 (0.34)
Insertion	0.00	0.00	0.08 (0.16)	0.20 (0.23)	0.00	0.11 (0.17)
Complex mutation	0.14 (0.31)	0.00	0.04 (0.08)	0.00	0.18 (0.36)	0.12 (0.29)
Total	6.23 (2.98)	7.20 (2.21)	5.95 (1.54)	4.71 (1.13)	6.29 (5.37)	7.51 (1.91)*

Data are mean (SD) of mutation frequency data from 411 mutants recovered from the *gpt* assay after excluding 155 mutants considered siblings. Control mice of both sexes were grouped for this analysis. The mutation frequency of A:T-to-G:C transitions and G:C-to-T:A transversions was significantly elevated in female mice infected with *H. pylori* for 12 mo.
*$P < 0.05$.

Mutation analysis using the Spi$^-$ assay revealed that the frequency of deletion mutations in *gpt* of gastric tissue DNA was not significantly affected by *H. pylori* infection (Fig. 5). Analyses of 57 samples from 32 mice showed that Spi$^-$ mutant frequencies in infected mice (females at 6 MPI, $4.8 \pm 2.5 \times 10^{-6}$, $P = 0.09$; females at 12 MPI, $5.0 \pm 2.6 \times 10^{-6}$, $P = 0.30$; males at 6 MPI, $6.3 \pm 2.5 \times 10^{-6}$, $P = 0.87$; and males at 12 MPI, $5.2 \pm 1.4 \times 10^{-6}$, $P = 0.17$) were not significantly different from those of age-matched controls at either time point (all mice at 6 MPI, $2.9 \pm 1.3 \times 10^{-6}$; all mice at 12 MPI, $3.6 \pm 1.8 \times 10^{-6}$).

Current models of inflammation-driven carcinogenesis are based on chronic inflammation inducing mutations that lead to cancer (40, 41). Female mice at 6 MPI had more hyperplasia, epithelial defects, and dysplasia than infected males and age-matched controls, but this increase in pathologic findings was not accompanied by increased frequency of mutations. This was detected only in infected female mice at 12 MPI, which had experienced more severe gastritis for a longer period, suggesting that gastritis is necessary but not sufficient to induce mutagenesis. Similarly, duration of infection in itself was insufficient, as mutation frequency was not increased in male mice at 12 MPI. Based on the GHAI, infected male mice had a weaker response at 6 MPI compared with infected females, whereas by 12 MPI, the level of pathologic process was similar in both sexes. These data suggest that the delayed onset of severe gastric lesions in males reduced the duration of their exposure to chronic gastritis, protecting them from mutagenesis, highlighting the importance of severity and duration of the inflammatory response.

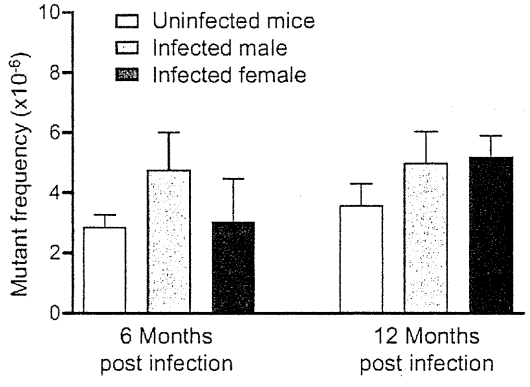

Fig. 5. Mutant frequency of deletions was unchanged by *H. pylori* infection. *H. pylori* infection did not alter the levels of deletions detected by the Spi$^-$ assay in uninfected mice (white bars; 6 MPI, n = 12; 12 MPI, n = 16), *H. pylori*-infected males (light gray bars; 6 MPI, n = 3; 12 MPI, n = 5) and *H. pylori*-infected females (dark gray bars; 6 MPI, n = 9; 12 MPI, n = 12). Control mice of both sexes were grouped for this analysis. Data are mean (SEM) of mutant frequency of mice in different treatment groups.

Our findings agree with current paradigms for the role of inflammation in carcinogenesis (4) and with the more severe pathology induced in female versus male C57BL/6 mice infected with *Helicobacter* spp. (42). Our observations in female *gpt* delta mice are consistent with previously reported data from female C57BL/6 Big Blue mice infected with *H. felis*, which induces more severe gastritis at earlier time points than *H. pylori*, effectively increasing the amount of DNA damage inflicted after infection (23, 43, 44). The higher mutation frequency found at 7 MPI in *H. felis*-infected female C57BL/6 Big Blue mice may be comparable to that occurring at 12 MPI in female *gpt* delta mice infected with *H. pylori*, based on increased inflammation and epithelial proliferation. In contrast, another study of DNA point mutations induced by *H. pylori* in male Big Blue mice reported that, although mutant frequency was increased at 6 MPI, it returned to control levels by 12 MPI (22). The decrease between 6 and 12 MPI was accompanied by loss of *iNOS* expression and reversion of the mutation spectrum to one indistinguishable from that of uninfected mice (22). Two possible explanations for these results are that (*i*) the increase in mutations at 6 MPI may have reflected jackpot mutations, because clonal expansion was not assessed or (*ii*) loss of infection resulted in absence of iNOS expression and reversion of the mutation spectrum. An additional factor pertinent to comparisons of previous mutagenesis studies involving gastric infection by *Helicobacter* spp. is the endogenous *Helicobacter* status of the mouse colony (45). We recently reported that concurrent, subclinical infection in C57BL/6 mice with non-gastric *Helicobacter bilis* significantly reduced *H. pylori*-associated premalignant gastric lesions at 6 and 11 MPI (46). This immunomodulatory effect could affect observed mutagenic responses,

and it is unknown whether Big Blue mice used in previous studies were free of enteric *Helicobacter* spp.

Our observed sex-based effects on mutagenesis induced by *H. pylori* in mice has not been reported previously, but sex bias has been found in other responses to infection. In *H. pylori*–infected Mongolian gerbils, immune responses and cytokine production were reported to be affected by sex (47), and *H. pylori* preferentially induced cancer in male INS-GAS mice (48). Greater female susceptibility to gastric *Helicobacter* infections has been noted previously in WT C57BL/6 mice (42), whereby females infected with *H. felis* experience an earlier onset of gastric inflammation, epithelial hyperplasia, atrophy, and apoptosis (42). Mechanisms responsible for the observed sex-based effects are incompletely understood, but findings to date collectively indicate that sex is an important variable, affecting strength of the host response to *H. pylori* infection, which in turn determines disease outcome.

The typical host response to *Helicobacter* infection is a proinflammatory Th1 response that causes chronic gastritis (49, 50). However, mouse strains such as BALB/c, which mount a strong antiinflammatory Th2 humoral immune response to *H. pylori* infection, develop less severe disease (51). We have previously shown that modulation of the Th1 response by an increased Th2 response reduces pathology associated with concurrent helminth infections (27). In the current study, the immune response of females to *H. pylori* infection was biased toward a greater Th1/Th2 ratio compared with males at both 6 and 12 mo. Higher Th1/Th2 ratios reflect a stronger inflammatory response to *H. pylori* infection. Furthermore, proinflammatory Th17 cells and regulatory T cells have been recently shown to modulate host responses to *H. pylori* (52, 53). *H. pylori*-specific Th17 immunity, mediated by IL-17 (54), increases inflammation unless it is suppressed by regulatory T cells, which are up-regulated by TGF-β and IL-10 (53). Higher levels of inflammation, epithelial defects, and atrophy were indeed observed in infected females at 6 MPI. At 12 MPI, the level of serum IgG2c was significantly elevated in infected females, reflective of increased proinflammatory cytokines in the gastric mucosa, and is consistent with the reduction in *H. pylori* colonization levels. The earlier onset of severe pathologic process caused by the Th1- and Th17-biased response to *H. pylori* was also associated with the increase in point mutations seen at 12 MPI.

In summary, we have shown that chronic *H. pylori* infection can cause premalignant gastric lesions and induce point mutations consistent with inflammatory processes. As our data are derived from analysis of nontranscribed DNA, it serves as an indicator of unbiased mutations reflecting genetic changes during the early stages of tumor initiation in inflamed tissues. At 12 mo, *H. pylori*-infected female C57BL/6 mice accumulate more inflammation-mediated point mutations compared with males as a result of a greater Th1-biased response to infection inducing earlier and more severe pathology. The sex-biased increase in premalignant gastric lesions and induction of mutations highlights the importance of taking into account sex-based effects in future studies of inflammation-driven disease.

Materials and Methods

Bacteria and Animals. *H. pylori* strain SS1 was grown on blood agar or *Brucella* broth with 5% FBS as described in *SI Materials and Methods*. Specific pathogen-free (including *Helicobacter* spp.) male and female C57BL/6 *gpt* delta mice (24) were infected by oral gavage with *H. pylori* SS1 or sham-dosed. At the indicated times, mice were euthanized, gastric tissue collected for histopathology and DNA and RNA extraction, and sera were collected for cytokine and Ig analysis. Gastric lesions were scored for inflammation, epithelial defects, atrophy, hyperplasia, mucous metaplasia, hyalinosis, intestinal metaplasia, and dysplasia using previously published criteria (55). The GHAI is the sum of inflammation, epithelial defects, atrophy, hyperplasia, intestinal metaplasia, and dysplasia scores. A detailed description of the husbandry, treatment, and histopathology is provided in *SI Materials and Methods*.

DNA Isolation and in Vitro Packaging. Genomic DNA was extracted from gastric tissue using RecoverEase DNA Isolation Kit (Stratagene) following the manufacturer's recommendations. λ-EG10 phages were packaged in vitro from genomic DNA using the Transpack Packaging Extract (Stratagene) following the instructions.

***gpt* Assay and Sequencing Analysis.** The 6-TG selection assay was performed as previously described (24, 56). Briefly, phages rescued from murine genomic DNA were transfected into *E. coli* YG6020 expressing Cre recombinase. Infected cells were cultured on plates containing chloramphenicol (Cm) and 6-TG for 3 d until 6-TG–resistant colonies appeared. To confirm the 6-TG–resistant phenotype, colonies were restreaked on plates containing Cm and 6-TG. Confirmed 6-TG–resistant colonies were cultured, and a 739-bp DNA product containing the *gpt* gene was amplified by PCR. DNA sequencing of the *gpt* gene was performed by the Biopolymers Facility at Harvard Medical School (Boston, MA) with AMPure beads (Agencourt) and a 3730xL DNA Analyzer (Applied Biosystems). Sequences were aligned with the *E. coli gpt* gene (GenBank M13422.1) (57) using Geneious (Biomatters). Mutations were classified as transitions, transversions, deletions, insertions, or complex (multiple changes). Duplicate mutations at the same site within an individual tissue were excluded to account for clonal expansion of sibling mutations. More information on primers and methods is provided in *SI Materials and Methods*.

Spi⁻ Assay. The Spi⁻ assay was performed as described in *SI Materials and Methods*. Briefly, phages rescued from murine genomic DNA were transfected into *E. coli* strains with or without P2 lysogen. Infected cells were cultured overnight on λ-trypticase agar plates to allow plaque formation. The inactivation of *red* and *gam* genes was confirmed by respotting plaques on another *E. coli* strain with P2 lysogen (24).

mRNA Expression. RNA was extracted from gastric tissue and reverse-transcribed to cDNA. Quantitative real-time PCR was performed using TaqMan Gene Expression Assays (Applied Biosystems). TaqMan primers and analysis methods are described in *SI Materials and Methods*.

***H. pylori* Detection.** *H. pylori* levels in the gastric mucosa were quantified by real-time quantitative PCR assay of gastric DNA as described in *SI Materials and Methods*. A threshold of 15 copies of the *H. pylori* genome was set as the lower limit for a positive sample.

Serum IgG Isotype Measurement. Sera were analyzed for *H. pylori*-specific IgG2c and IgG1 by ELISA. Additional information on the measurements is provided in *SI Materials and Methods*.

Statistical Analysis. Two-way ANOVA followed by Bonferroni posttests were used to analyze GHAI and mRNA expression values. Student two-tailed *t* tests were used to analyze mutant and mutation frequency data and serum IgG isotypes. Poisson distribution analysis was used to determine hotspots at a 99% confidence level (58). For some analyses, age-matched controls of both sexes were grouped when no statistical differences were detected between sexes. Analyses were done with GraphPad Prism, version 4.0, or Microsoft Excel 2002. $P < 0.05$ was considered significant.

ACKNOWLEDGMENTS. We thank Sureshkumar Muthupalani for help with the histological images and Laura J. Trudel for assistance with the manuscript and figures. This study is dedicated in loving memory of David Schauer, a mentor and a friend, for his contribution in the design and analysis of this work. This work was supported by National Institutes of Health Grants R01-AI037750 and P01-CA026731 and Massachusetts Institute of Technology Center for Environmental Health Sciences Program Project Grant P30-ES02109.

1. Fox JG, Wang TC (2007) Inflammation, atrophy, and gastric cancer. *J Clin Invest* 117: 60–69.
2. Suerbaum S, Michetti P (2002) Helicobacter pylori infection. *N Engl J Med* 347:1175–1186.
3. International Agency for Research on Cancer (1994) Schistosomes, liver flukes and Helicobacter pylori. IARC Working Group on the Evaluation of Carcinogenic Risks to Humans. Lyon, 7-14 June 1994. *IARC Monogr Eval Carcinog Risks Hum* 61:1–241.
4. Coussens LM, Werb Z (2002) Inflammation and cancer. *Nature* 420:860–867.
5. Obst B, Wagner S, Sewing KF, Beil W (2000) Helicobacter pylori causes DNA damage in gastric epithelial cells. *Carcinogenesis* 21:1111–1115.
6. Xu H, et al. (2004) Spermine oxidation induced by Helicobacter pylori results in apoptosis and DNA damage: Implications for gastric carcinogenesis. *Cancer Res* 64: 8521–8525.

7. Davies GR, et al. (1994) Relationship between infective load of Helicobacter pylori and reactive oxygen metabolite production in antral mucosa. *Scand J Gastroenterol* 29: 419–424.
8. Davies GR, et al. (1994) Helicobacter pylori stimulates antral mucosal reactive oxygen metabolite production in vivo. *Gut* 35:179–185.
9. Mannick EE, et al. (1996) Inducible nitric oxide synthase, nitrotyrosine, and apoptosis in Helicobacter pylori gastritis: Effect of antibiotics and antioxidants. *Cancer Res* 56: 3238–3243.
10. Meira LB, et al. (2008) DNA damage induced by chronic inflammation contributes to colon carcinogenesis in mice. *J Clin Invest* 118:2516–2525.
11. Nair J, et al. (2006) Increased etheno-DNA adducts in affected tissues of patients suffering from Crohn's disease, ulcerative colitis, and chronic pancreatitis. *Antioxid Redox Signal* 8:1003–1010.
12. Zhuang JC, Lin C, Lin D, Wogan GN (1998) Mutagenesis associated with nitric oxide production in macrophages. *Proc Natl Acad Sci USA* 95:8286–8291.
13. Sato Y, et al. (2006) IL-10 deficiency leads to somatic mutations in a model of IBD. *Carcinogenesis* 27:1068–1073.
14. Bartsch H, Nair J (2004) Oxidative stress and lipid peroxidation-derived DNA-lesions in inflammation driven carcinogenesis. *Cancer Detect Prev* 28:385–391.
15. Nair U, Bartsch H, Nair J (2007) Lipid peroxidation-induced DNA damage in cancer-prone inflammatory diseases: a review of published adduct types and levels in humans. *Free Radic Biol Med* 43:1109–1120.
16. Kang JM, Iovine NM, Blaser MJ (2006) A paradigm for direct stress-induced mutation in prokaryotes. *FASEB J* 20:2476–2485.
17. Crabtree JE, Ferrero RL, Kusters JG (2002) The mouse colonizing Helicobacter pylori strain SS1 may lack a functional cag pathogenicity island. *Helicobacter* 7:139–140, author reply 140–141.
18. Lee A, Mitchell H, O'Rourke J (2002) The mouse colonizing Helicobacter pylori strain SS1 may lack a functional cag pathogenicity island: Response. *Helicobacter* 7:140–141.
19. Miyazawa M, et al. (2003) Suppressed apoptosis in the inflamed gastric mucosa of *Helicobacter pylori*-colonized iNOS-knockout mice. *Free Radic Biol Med* 34:1621–1630.
20. Jang J, et al. (2003) Malgun (clear) cell change in *Helicobacter pylori* gastritis reflects epithelial genomic damage and repair. *Am J Pathol* 162:1203–1211.
21. Lee H, et al. (2000) "Malgun" (clear) cell change of gastric epithelium in chronic *Helicobacter pylori* gastritis. *Pathol Res Pract* 196:541–551.
22. Touati E, et al. (2003) Chronic Helicobacter pylori infections induce gastric mutations in mice. *Gastroenterology* 124:1408–1419.
23. Jenks PJ, Jeremy AH, Robinson PA, Walker MM, Crabtree JE (2003) Long-term infection with Helicobacter felis and inactivation of the tumour suppressor gene p53 cumulatively enhance the gastric mutation frequency in Big Blue transgenic mice. *J Pathol* 201:596–602.
24. Nohmi T, et al. (1996) A new transgenic mouse mutagenesis test system using Spi- and 6-thioguanine selections. *Environ Mol Mutagen* 28:465–470.
25. Ihrig M, Whary MT, Dangler CA, Fox JG (2005) Gastric helicobacter infection induces a Th2 phenotype but does not elevate serum cholesterol in mice lacking inducible nitric oxide synthase. *Infect Immun* 73:1664–1670.
26. Lee CW, et al. (2008) Helicobacter pylori eradication prevents progression of gastric cancer in hypergastrinemic INS-GAS mice. *Cancer Res* 68:3540–3548.
27. Fox JG, et al. (2000) Concurrent enteric helminth infection modulates inflammation and gastric immune responses and reduces helicobacter-induced gastric atrophy. *Nat Med* 6:536–542.
28. De Bont R, van Larebeke N (2004) Endogenous DNA damage in humans: A review of quantitative data. *Mutagenesis* 19:169–185.
29. Burney S, Caulfield JL, Niles JC, Wishnok JS, Tannenbaum SR (1999) The chemistry of DNA damage from nitric oxide and peroxynitrite. *Mutat Res* 424:37–49.
30. Kadlubar FF, et al. (1998) Comparison of DNA adduct levels associated with oxidative stress in human pancreas. *Mutat Res* 405:125–133.
31. Pandya GA, Moriya M (1996) 1, N6-ethenodeoxyadenosine, a DNA adduct highly mutagenic in mammalian cells. *Biochemistry* 35:11487–11492.
32. Ambs S, et al. (1999) Relationship between p53 mutations and inducible nitric oxide synthase expression in human colorectal cancer. *J Natl Cancer Inst* 91:86–88.
33. Kim MY, Wogan GN (2006) Mutagenesis of the supF gene of pSP189 replicating in AD293 cells cocultivated with activated macrophages: roles of nitric oxide and reactive oxygen species. *Chem Res Toxicol* 19:1483–1491.
34. Dedon PC, Plastaras JP, Rouzer CA, Marnett LJ (1998) Indirect mutagenesis by oxidative DNA damage: formation of the pyrimidopurinone adduct of deoxyguanosine by base propenal. *Proc Natl Acad Sci USA* 95:11113–11116.
35. Jackson AL, Loeb LA (2001) The contribution of endogenous sources of DNA damage to the multiple mutations in cancer. *Mutat Res* 477:7–21.
36. Wood ML, Esteve A, Morningstar ML, Kuziemko GM, Essigmann JM (1992) Genetic effects of oxidative DNA damage: comparative mutagenesis of 7,8-dihydro-8-oxoguanine and 7,8-dihydro-8-oxoadenine in Escherichia coli. *Nucleic Acids Res* 20: 6023–6032.
37. Pang B, et al. (2007) Lipid peroxidation dominates the chemistry of DNA adduct formation in a mouse model of inflammation. *Carcinogenesis* 28:1807–1813.
38. Masumura K, et al. (2003) Low dose genotoxicity of 2-amino-3,8-dimethylimidazo[4,5-f]quinoxaline (MeIQx) in gpt delta transgenic mice. *Mutat Res* 541:91–102.
39. Masumura K, et al. (2000) Characterization of mutations induced by 2-amino-1-methyl-6-phenylimidazo[4,5-b]pyridine in the colon of gpt delta transgenic mouse: novel G:C deletions beside runs of identical bases. *Carcinogenesis* 21:2049–2056.
40. Balkwill F, Coussens LM (2004) Cancer: An inflammatory link. *Nature* 431:405–406.
41. Clevers H (2004) At the crossroads of inflammation and cancer. *Cell* 118:671–674.
42. Court M, Robinson PA, Dixon MF, Jeremy AH, Crabtree JE (2003) The effect of gender on Helicobacter felis-mediated gastritis, epithelial cell proliferation, and apoptosis in the mouse model. *J Pathol* 201:303–311.
43. Fox JG, et al. (2002) Germ-line p53-targeted disruption inhibits helicobacter-induced premalignant lesions and invasive gastric carcinoma through down-regulation of Th1 proinflammatory responses. *Cancer Res* 62:696–702.
44. Lee A, Fox JG, Otto G, Murphy J (1990) A small animal model of human Helicobacter pylori active chronic gastritis. *Gastroenterology* 99:1315–1323.
45. Taylor NS, et al. (1995) Long-term colonization with single and multiple strains of Helicobacter pylori assessed by DNA fingerprinting. *J Clin Microbiol* 33:918–923.
46. Lemke LB, et al. (2009) Concurrent Helicobacter bilis infection in C57BL/6 mice attenuates proinflammatory *H. pylori*-induced gastric pathology. *Infect Immun* 77: 2147–2158.
47. Crabtree JE, et al. (2004) Gastric mucosal cytokine and epithelial cell responses to Helicobacter pylori infection in Mongolian gerbils. *J Pathol* 202:197–207.
48. Fox JG, et al. (2003) Host and microbial constituents influence Helicobacter pylori-induced cancer in a murine model of hypergastrinemia. *Gastroenterology* 124:1879–1890.
49. Bamford KB, et al. (1998) Lymphocytes in the human gastric mucosa during Helicobacter pylori have a T helper cell 1 phenotype. *Gastroenterology* 114:482–492.
50. Mohammadi M, Czinn S, Redline R, Nedrud J (1996) Helicobacter-specific cell-mediated immune responses display a predominant Th1 phenotype and promote a delayed-type hypersensitivity response in the stomachs of mice. *J Immunol* 156: 4729–4738.
51. Sakagami T, et al. (1996) Atrophic gastric changes in both Helicobacter felis and Helicobacter pylori infected mice are host dependent and separate from antral gastritis. *Gut* 39:639–648.
52. Lee CW, et al. (2007) Wild-type and interleukin-10-deficient regulatory T cells reduce effector T-cell-mediated gastroduodenitis in Rag2-/- mice, but only wild-type regulatory T cells suppress Helicobacter pylori gastritis. *Infect Immun* 75:2699–2707.
53. Kao JY, et al. (2010) Helicobacter pylori immune escape is mediated by dendritic cell-induced Treg skewing and Th17 suppression in mice. *Gastroenterology* 138:1046–1054.
54. Xu S, Cao X (2010) Interleukin-17 and its expanding biological functions. *Cell Mol Immunol* 7:164–174.
55. Rogers AB, et al. (2005) Helicobacter pylori but not high salt induces gastric intraepithelial neoplasia in B6129 mice. *Cancer Res* 65:10709–10715.
56. Masumura K, et al. (1999) Spectra of gpt mutations in ethylnitrosourea-treated and untreated transgenic mice. *Environ Mol Mutagen* 34:1–8.
57. Nüesch J, Schümperli D (1984) Structural and functional organization of the gpt gene region of Escherichia coli. *Gene* 32:243–249.
58. Kim MY, Dong M, Dedon PC, Wogan GN (2005) Effects of peroxynitrite dose and dose rate on DNA damage and mutation in the supF shuttle vector. *Chem Res Toxicol* 18: 76–86.

TOXICOLOGICAL SCIENCES 114(1), 71–78 (2010)
doi:10.1093/toxsci/kfp306
Advance Access publication December 21, 2009

Integration of *In Vivo* Genotoxicity and Short-term Carcinogenicity Assays Using F344 *gpt* Delta Transgenic Rats: *In Vivo* Mutagenicity of 2,4-Diaminotoluene and 2,6-Diaminotoluene Structural Isomers

Naomi Toyoda-Hokaiwado,*[,2] Tomoki Inoue,†[,2] Kenichi Masumura,* Hiroyuki Hayashi,‡ Yuji Kawamura,‡ Yasushi Kurata,‡ Makiko Takamune,* Masami Yamada,* Hisakazu Sanada,§ Takashi Umemura,† Akiyoshi Nishikawa,† and Takehiko Nohmi*[,1]

*Division of Genetics and Mutagenesis and †Division of Pathology, National Institute of Health Sciences, Setagaya-ku, Tokyo 158-8501, Japan; ‡Meiji Seika Kaisha, Ltd, Kohoku-ku, Yokohama, Kanagawa 222-8567, Japan; and §Safety Research Department, Central Research Laboratories, Kaken Pharmaceutical Co., Ltd, Fujieda, Shizuoka 426-8646, Japan

[1] To whom correspondence should be addressed at Division of Genetics and Mutagenesis, 1-18-1 Kamiyoga, Setagaya-ku, Tokyo 158-8501, Japan. Fax: +81-3-3700-2348. E-mail: nohmi@nihs.go.jp.
[2] These authors contributed to this work equally.

Received October 16, 2009; accepted December 15, 2009

An important trend in current toxicology is the replacement, reduction, and refinement of the use of experimental animals (the 3R principle). We propose a model in which *in vivo* genotoxicity and short-term carcinogenicity assays are integrated with F344 *gpt* delta transgenic rats. Using this model, the genotoxicity of chemicals can be identified in target organs using a shuttle vector λ EG10 that carries reporter genes for mutations; short-term carcinogenicity is determined by the formation of glutathione *S*-transferase placenta form (GST-P) foci in the liver. To begin validating this system, we examined the genotoxicity and hepatotoxicity of structural isomers of 2,4-diaminotoluene (2,4-DAT) and 2,6-diaminotoluene (2,6-DAT). Although both compounds are genotoxic in the Ames/*Salmonella* assay, only 2,4-DAT induces tumors in rat livers. Male F344 *gpt* delta rats were fed diet containing 2,4-DAT at doses of 125, 250, or 500 ppm for 13 weeks or 2,6-DAT at a dose of 500 ppm for the same period. The mutation frequencies of base substitutions, mainly at G:C base pairs, were significantly increased in the livers of 2,4-DAT–treated rats at all three doses. In contrast, virtually no induction of genotoxicity was identified in the kidneys of 2,4-DAT–treated rats or in the livers of 2,6-DAT–treated rats. GST-P–positive foci were detected in the livers of rats treated with 2,4-DAT at a dose of 500 ppm but not in those treated with 2,6-DAT. Integrated genotoxicity and short-term carcinogenicity assays may be useful for early identifying genotoxic and nongenotoxic carcinogens in a reduced number of experimental animals.

Key Words: ***gpt* delta transgenic rat; diaminotoluenes; genotoxicity; carcinogenicity; 3R principle.**

Transgenic rodent models have advanced the field of *in vivo* genotoxicity studies (Nohmi and Masumura, 2005; Nohmi *et al.*, 2000). In these models, λ phage DNA carrying reporter genes for mutations are integrated into the chromosomes of transgenic rodents; the phage DNA is retrieved in phage particles by *in vitro* packaging reactions. The rescued phages are introduced into *Escherichia coli* cells, and mutants that were generated in the rodents are selected. With the shuttle vector system, one can examine the mutagenicity of chemicals in any rodent organ or tissues, including germ cells (Eastmond *et al.*, 2009; Hashimoto *et al.*, 2009). In addition, the mutants recovered from the rodents can be characterized by DNA sequencing (Heddle *et al.*, 2000). Transgenic genotoxicity assays are a reliable method for determining whether genotoxicity is involved in chemical carcinogenicity in the target organs of rodents (Thybaud *et al.*, 2003).

In 1996, we developed the novel transgenic mouse *gpt* delta for *in vivo* genotoxicity assays (Nohmi *et al.*, 1996). These mice have approximately 80 copies of λ EG10 DNA at a single site in chromosome 17 of C57 BL/6J mice (Masumura *et al.*, 1999). A feature of this transgenic mouse is that two mutant selections can be performed instead of just one, to identify a wider spectrum of *in vivo* mutations: *gpt* selection to identify point mutations such as base substitutions and frameshift mutations and Spi$^-$ selection to identify deletion mutations. Because of their sensitivity to deletion-type mutations, *gpt* delta mice have been utilized for radiation biology, cancer research, and regulatory toxicology (Aoki *et al.*, 2007; Masumura *et al.*, 2002; Shibata *et al.*, 2009; Xu *et al.*, 2007). In 2003, we established *gpt* delta rats in a Sprague-Dawley (SD) background by introducing λ EG10 DNA into fertilized SD rat eggs (Hayashi *et al.*, 2003). This *gpt* delta rat carries approximately five copies of λ EG10 DNA at a single site in chromosome 4 and is sensitive to induction of point mutations and deletions by benzo[*a*]pyrene and potassium bromate (Hayashi *et al.*, 2003; Umemura *et al.*, 2009).

Here, we report the establishment of *gpt* delta rat in a Fischer 344 background by backcross of SD *gpt* delta rats with F344 rats for 15 generations. We generated F344 *gpt* delta rats because this background is frequently used for 2-year cancer bioassays. In addition, glutathione *S*-transferase placenta form (GST-P)–positive preneoplastic hepatic foci can be analyzed in the rats (Ito *et al.*, 2000). The results of bioassay using GST-P–positive foci show good correlation with those of 2-year cancer bioassay (Ito *et al.*, 2000; Ogiso *et al.*, 1985). Therefore, GST-P–positive foci formation assay was used as short-term carcinogenicity assay in this study. We hypothesized that we could integrate a genotoxicity assay with a short-term carcinogenicity assay utilizing GST-P foci in F344 *gpt* delta rats. This would reduce the number of animals required for both assays and would allow for examination of the relationship between genotoxicity and preneoplastic lesion formation within the same organs and tissues of chemically treated F344 *gpt* delta rats.

To begin validating this system, we examined the *in vivo* genotoxicity and hepatotoxicity of 2,4-diaminotoluene (2,4-DAT) and 2,6-diaminotoluene (2,6-DAT). The first chemical, 2,4-DAT, is used as an intermediate of the production of toluene diisocyanate, which is a monomer for the production of polyurethane, while 2,6-DAT is an intermediate of dyes, rubber chemicals, and various polymers (NTP 1979, 1980). Although both are genotoxic *in vitro* (Cunningham *et al.*, 1989), only 2,4-DAT is carcinogenic in the livers of female mice and male and female rats (NTP, 1979). 2,4-DAT also induces lymphoma in female mice and mammary and subcutaneous tumors in rats. 2,6-DAT is not carcinogenic in mice and rats, regardless of their sex (NTP, 1980). Previous studies with MutaMouse (Kirkland and Beevers, 2006) and Big Blue mouse (Cunningham *et al.*, 1996) indicate that 2,4-DAT is mutagenic in the liver, while 2,6-DAT is not. However, the transgenic mice employed for these studies were males, in which the hepatocarcinogenicity of 2,4-DAT is not observed. In addition, there are no reports on *in vivo* gene mutations in rats. Thus, we decided to examine the *in vivo* genotoxicity of both compounds in the liver, as carcinogenic target organ of 2,4-DAT, and kidney, as non-carcinogenic target, along with immunohistochemical analyses. We chose 500 ppm as the highest dose for both DATs according to the dose used in the National Toxicology Program 2-year cancer bioassay (NTP, 1979, 1980). We treated the rats with chemicals for 13 weeks because this period is customarily used to determine the appropriate doses for 2-year cancer bioassays; furthermore, shorter term treatments (e.g., treatments with potassium bromate for 5 weeks [Umemura *et al.*, 2006]), sometimes do not induce detectable mutations *in vivo*.

MATERIALS AND METHODS

Establishment of F344 gpt delta rats. All the animals were maintained at Japan SLC (Shizuoka, Japan). The F344 *gpt* delta transgenic rat strain was developed by backcrosses of the original SD *gpt* delta transgenic rat with wild-type F344 rats. In brief, male SD *gpt* delta transgenic rat was mated with F344 female rat to produce an F1 generation. Offspring from the F1 generation were mated with F344 rats to yield an F2 generation. All offspring from successive backcrosses were examined for the possession of the *gpt* gene by PCR (Hayashi *et al.*, 2003). After 15 successive backcrosses, identity of the resulting rats to F344 recipient is more than 99.9%. Thus, they were referred to as F344 *gpt* delta rats.

Chemicals. 2,4-DAT (purity 95%) and 2,6-DAT (purity 98%) were purchased from Wako Pure Chemical Industries (Osaka, Japan). Diethylnitrosamine (DEN) was obtained from Sigma-Aldrich Japan (Tokyo, Japan).

Bacterial reverse mutation test (Ames test). The mutagenic activities of 2,4-DAT and 2,6-DAT were assayed in a bacterial reverse mutation assay using *Salmonella typhimurium* tester strains TA98 and YG1024, an *O*-acetyltransferase (OAT)–overexpressing derivative. The test was conducted by the preincubation method (Maron and Ames, 1983) in the presence or the absence of S9 mix. At least two plates were used for each dose, and the mean values of the number of revertants per plate were calculated. Chemicals were dissolved in dimethyl sulfoxide, which was used as the negative control.

Animals, diet, and housing conditions. Male 6-week-old F344 *gpt* delta transgenic rats were obtained from Japan SLC and housed five animals per polycarbonate cage under specific pathogen-free standard laboratory conditions: room temperature, 23°C ± 2°C; relative humidity, 60 ± 5%; with a 12:12-h light-dark cycle; and free access to CRF-1 basal diet (Oriental Yeast Company, Tokyo, Japan) and tap water. After a 1-week acclimation period, the animals were used for the experiments.

Treatments of animals. The protocol for this study was approved by the Animal Care and Utilization Committee of the National Institute of Health Sciences. Thirty male F344 *gpt* delta rats were randomized by weight into six groups. 2,4-DAT and 2,6-DAT were each mixed into Oriental CRF-1 powdered basal diet (Oriental Yeast Company) and stored at 4°C in the dark before use. Starting at 7 weeks of age, the rats were fed diets containing 0, 125, 250, or 500 ppm 2,4-DAT or 500 ppm 2,6-DAT for 13 weeks. There was also a positive control group; these rats were received a once-a-week ip injection of 20 mg/kg body weight DEN for 13 weeks. Parameters monitored included clinical signs, body weight, and food intake. The highest dose of 2,4-DAT was reduced from 500 to 400 ppm at week 9 because the dose at 500 ppm reduced the body weight of rats at week 8. All the surviving animals were killed under ether anesthesia at the end of the experiments. The liver and kidneys were isolated from each animal and were immediately excised, weighed, and cut into 2- to 3-mm-thick slices. The slices were fixed in 10% buffered formalin solution and routinely processed to paraffin blocks for histopathological examination as well as immunohistochemistry. Hematoxylin and eosin-stained tissue preparations cut from the blocks were examined by light microscopy.

Micronucleus assay. At autopsy, 60 µl of peripheral blood was obtained from the tail veins of all animals. The samples were processed according to the instructions supplied with the MicroFlow^{PLUS} kit (Litron, Rochester, NY), fixed in ultra-cold methanol, and stored immediately after fixation at −80°C until flow cytometry analysis was performed. Approximately 20,000 reticulocytes were counted for each sample using Becton-Dickinson FACSCalibur flow cytometer (Franslin Lakes, NJ) to detect the presence of micronuclei (MNs).

Immunohistochemical procedures. Liver sections of 3-µm thickness were treated with rabbit anti-rat GST-P antibody (1:1000; Medical & Biological Laboratories, Nagoya, Japan) and monoclonal mouse anti-Ki67 (MIB-5) antibody (1:50; Dako, Tokyo, Japan) (1:50), respectively. Areas and numbers of GST-P–positive foci larger than 0.1 mm in diameter of the liver sections were quantitatively measured with an image processor for analytical pathology (IPAP-WIN; Sumika Technos Company, Osaka, Japan). To investigate proliferative activity, we counted at least 1000 hepatocyte nuclei in each liver; labeling indices were calculated as the percentage of cells positive for Ki67

staining. The remaining tissues were immediately frozen in liquid nitrogen and stored at −80°C for subsequent mutation assays.

DNA isolation and in vitro packaging of λ phage DNA. High–molecular-weight genomic DNA was extracted from the liver and kidneys using the RecoverEase DNA Isolation kit (Stratagene, La Jolla, CA). λ EG10 phages were rescued using Transpack Packaging Extract (Stratagene).

gpt Mutation assay. The assay was conducted according to previously published methods (Nohmi *et al.*, 1996). All the confirmed *gpt* mutants recovered from the livers were sequenced; identical mutations from the same rat were counted as one mutant. The mutant frequencies of the *gpt* gene (*gpt* MFs) in the liver and kidney were calculated by dividing the number of confirmed 6-thioguanine–resistant colonies by the number of rescued plasmids. DNA sequencing of the *gpt* gene was performed with the BigDye Terminater Cycle Sequencing Ready Reaction (Applied Biosystems, Foster City, CA) on an ABI PRISM 310 Genetic Analyzer (Applied Biosystems).

Spi⁻ assay. The Spi⁻ assay was conducted according to previously published methods (Masumura *et al.*, 2002). To confirm the Spi⁻ phenotype of the candidates, suspensions were spotted on three types of plates on which XL-1 Blue MRA, XL-1 Blue MRA P2, or WL95 P2 strains were spread with soft agar. True Spi⁻ mutants, which made clear plaques on all of the plates, were counted. Spi⁻ mutant lysates were obtained by infecting *E. coli* LE392 with the recovered Spi⁻ mutants. The lysates were used as templates for PCR and sequencing analysis to determine the deleted regions (Masumura *et al.*, 2002). The Spi⁻ mutants were categorized into three classes: one base pair (bp) deletions, deletions of more than 1 bp, and complex mutations. The entire sequence of λ EG10 is available at http://dgm2alpha.nihs.go.jp/default.htm.

Statistical analysis. The statistical significance of the difference in the value of MFs between treated groups and negative controls was analyzed by Student's *t*-test. A p value less than 0.05 denoted the presence of a statistically significant difference. Variances in values for body weight, organ weight, and immunohistochemical data were examined by one-way ANOVA with Dunnett's multiple test to compare the differences between control and treated groups.

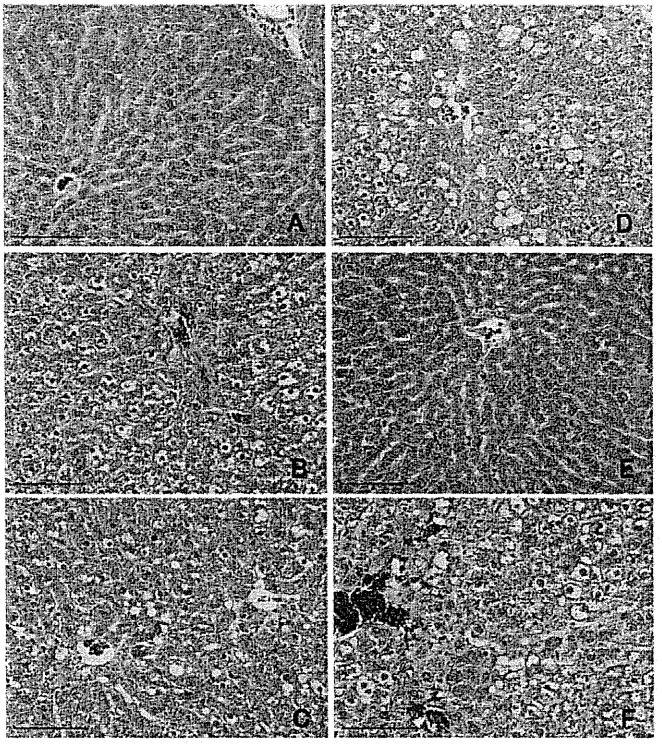

FIG. 1. Histological comparison of rat livers treated with 0 ppm 2,4-DAT (A), 125 ppm 2,4-DAT (B), 250 ppm 2,4-DAT (C), 500 ppm 2,4-DAT (D), 500 ppm 2,6-DAT (E), and DEN (F). Hepatotoxicity was observed in rats administered 2,4-DAT and DEN. Bar = 100 μm.

RESULTS

Dietary Treatment with 2,4-DAT Induced Preneoplastic Lesions in the Livers of F344 gpt Delta Rats

Dietary treatment with 2,4-DAT reduced body weight significantly at all three doses, while dietary treatment with 2,6-DAT did not (Supplementary table 1). Treatments with 2,4-DAT, but not 2,6-DAT, increased the relative weight of the livers and kidneys in a dose-dependent manner. Hypertrophy and vacuolar degeneration of hepatocytes was observed in the livers of rats in the 2,4-DAT treatment groups (Fig. 1). Cell proliferation was significantly enhanced by 2,4-DAT at a dose of 250 ppm but not by treatment with 2,6-DAT or other doses of 2,4-DAT (Table 1). That labeling index was twofold higher compared with that of basal diet group. GST-P–positive foci were induced by treatment with 2,4-DAT at a dose of 250 or 500 ppm and by the positive control treatment with DEN (Table 2). There were significant differences in number of foci and area of foci between rats treated with 2,4-DAT at 500 ppm and those of the basal diet group and between rats treated with DEN and the control group. No histopathological changes were observed in the kidneys of rats that were fed 2,4-DAT or 2,6-DAT. These results suggest that 2,4-DAT, but not 2,6-DAT, induced preneoplastic lesions in the livers of F344 *gpt* delta rats.

Both 2,4-DAT and 2,6-DAT Induced Mutations In Vitro

We confirmed that both 2,4-DAT and 2,6-DAT were mutagenic in *S. typhimurium* strain TA98 in the presence of S9 activation (Fig. 2). Treating cells with either of the DATs in the absence of S9 mix did not produce any increase in the number of revertants per plate. Similar, but less significant, results were obtained with another standard *S. typhimurium* strain TA100 (Supplementary table 2). These observations suggest that DAT metabolites were responsible for the mutagenic effects. To explore the metabolic activation pathways *in vitro*, we employed strain YG1024, which overproduces OAT, a phase II enzyme. Strain YG1024 detects frameshift mutations because it was derived from strain TA98 (Watanabe *et al.*, 1994). As shown in Figure 2, YG1024 exhibited enhanced sensitivity to the mutagenicity of both 2,4-DAT and 2,6-DAT in the presence of S9 activation. The mutagenicity of 2,6-DAT was similar to that of 2,4-DAT in the presence of S9 activation (in strain TA98, 1036 vs. 1316 His^+ revertants per plate at 625 μg of 2,4-DAT and 2,6-DAT, respectively; in strain YG1024, 3460 vs. 3896 His^+ revertants per plate at 156 μg of 2,4-DAT and 2,6-DAT, respectively).

TABLE 1
Quantification of Hepatocyte Proliferation

	No. of Rats	No. of Total Nuclei	No. of Ki-67–Positive Nuclei	Index
Basal diet	5	2170.8 ± 890.9	27.4 ± 8.1	0.013 ± 0.004
Basal diet (DEN)	5	1749.6 ± 729.2[a]	73.8 ± 19.7	0.042 ± 0.009*
125 ppm 2,4-DAT	5	1700.2 ± 700.1[a]	14.0 ± 6.6	0.008 ± 0.005
250 ppm 2,4-DAT	5	1436.4 ± 596.7[a]	44.4 ± 10.5	0.031 ± 0.007*
500 ppm 2,4-DAT	5	1308.6 ± 537.6[a]	20.4 ± 9.0	0.015 ± 0.006
500 ppm 2,6-DAT	5	2048.8 ± 860.8	17.8 ± 7.4	0.014 ± 0.004

[a]Total number of nuclei was significantly decreased compared to the basal diet treatment group.
*Significantly different from the basal diet group ($p < 0.01$).

These results suggest that both DATs are mutagenic in the presence of S9 activation *in vitro* and also that *O*-acetylation is important for the metabolic activation.

In Vivo Mutagenicity of 2,4-DAT

For the initial *in vivo* genotoxicity assay, we examined MN formation in the peripheral blood of F344 *gpt* delta rats treated with 2,4-DAT or 2,6-DAT. However, no significant increase in MN frequency was observed in any of the treated groups (Supplementary table 4).

Next, we examined the mutagenicity of the DATs in the livers and kidneys of the rats. *gpt* MFs were significantly increased in the livers of 2,4-DAT–treated rats at all three doses and in the DEN-positive control, compared to the control group (Fig. 3, Supplementary table 3). No increases in MFs were observed in the livers of 2,6-DAT–treated rats or in the kidneys of either 2,4-DAT– or 2,6-DAT–treated rats. To characterize the *gpt* mutations in the liver, we performed DNA sequencing (Table 3). The predominant base substitutions were G:C-to-A:T transitions and G:C-to-T:A and G:C-to-C:G transversions in the 2,4-DAT–treated groups. In addition, base substitutions at A:T bps were also induced. In the DEN-treated positive control group, A:T-to-T:A transversions were the most predominant type of mutation. Spi^- MFs in the liver were also significantly increased in 2,4-DAT treatment groups at doses of 250 and 500 ppm and in the DEN-treated group (Table 4). They were not increased by treatment with 2,6-DAT. DNA sequence analysis revealed that the specific mutant frequency (SMF) of a −1 frameshift at run sequences such as GGGG in the *gam* gene was increased more than fourfold after treatment with 500 ppm 2,4-DAT, while the SMF of deletions of more than two bps was not enhanced at this dose (Supplementary table 5). Thus, most of the Spi^- mutations were −1 frameshift mutations at run sequences, and large deletion mutations were not significantly induced by treatment with 2,4-DAT.

TABLE 2
Quantification of GST-P–Positive Foci

	No. of Rats	No. of Foci (No./cm^2)	Area of Foci (mm^2/cm^2)
Basal diet	5	0.00 ± 0.00	0.000 ± 0.000
Basal diet (DEN)	5	78.92 ± 17.70**	1.924 ± 0.655**
125 ppm 2,4-DAT	5	0.00 ± 0.00	0.000 ± 0.000
250 ppm 2,4-DAT	5	1.19 ± 1.21	0.022 ± 0.023
500 ppm 2,4-DAT	5	6.05 ± 3.93*	0.502 ± 0.476*
500 ppm 2,6-DAT	5	0.00 ± 0.00	0.000 ± 0.000

*Significantly different from the basal diet group ($p < 0.05$).
**Significantly different from the basal diet group ($p < 0.01$).

DISCUSSION

In the regulatory sciences, a default assumption is that genotoxic carcinogens have no thresholds for their activities, and thus, no acceptable daily intake can be set for these chemicals when they are used as food additives, pesticides, or veterinary medicines (Kirsch-Volders *et al.*, 2000; Nohmi, 2008). It is thought that single molecules of genotoxic compounds can induce mutations, and thus, genotoxic carcinogens impose carcinogenic risks to humans even at very low doses. However, how the genotoxicity of chemicals should be defined is not entirely clear. Currently, more than 200 genotoxicity assays have been proposed (Preston and Hoffmann, 2007). Unsurprisingly, the results among the various genotoxicity assays are inconsistent. The aromatic amine structural isomers 2,4-DAT and 2,6-DAT are an interesting reference pair that illustrates the inconsistency between *in vitro* and *in vivo* results (Cunningham *et al.*, 1989). Both 2,4-DAT and 2,6-DAT are mutagenic *in vitro* in *S. typhimurium* strains, but only 2,4-DAT is carcinogenic in mice and rats (NTP, 1979).

In this study, we confirmed *in vitro* genotoxicity with *S. typhimurium* TA98 and YG1024 and explored *in vivo* genotoxicity with F344 *gpt* delta rats. Both DATs were mutagenic in the *S. typhimurium* strains *in vitro* when the S9 activation system was present (Fig. 2). In contrast, only 2,4-DAT was mutagenic in the livers of rats (Fig. 3, Table 4, Supplementary table 4). Both *gpt* and Spi^- MFs in the liver were significantly increased in 2,4-DAT–treated rats compared to those in the control group. We did not observe any increase in *gpt* MFs in the livers of 2,6-DAT–treated rats or in the kidneys of 2,4- or 2,6-DAT–treated rats (Fig. 3, Supplementary table 4). Kidney may not have capacity to activate 2,4-DAT as in the case of bone marrow (see below). We identified preneoplastic lesions (i.e., GST-P–positive foci) in the livers of rats treated with 250 and 500 ppm 2,4-DAT (Table 2) but not in the livers of rats treated with 2,6-DAT. Generally, proliferation is activated in cancer cells. Ki-67 is a nuclear marker of cell proliferation and detectable in cells at all phases of the cell cycles except G_0 (Gerdes *et al.*, 1983). The Ki-67

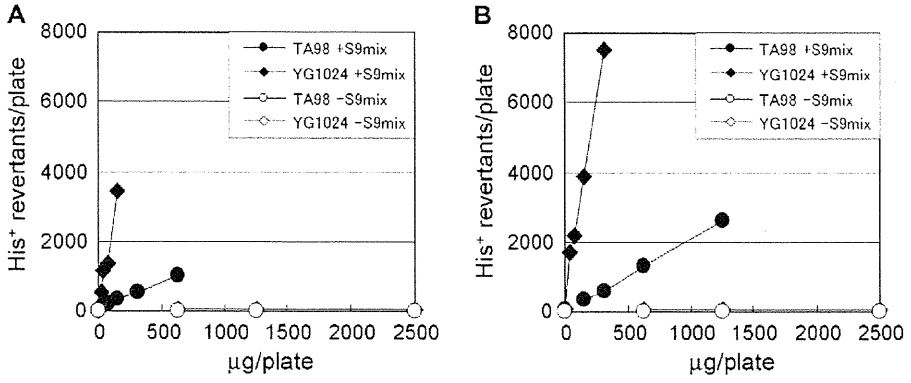

FIG. 2. Mutagenic activity of 2,4-DAT (A) and 2,6-DAT (B) in *Salmonella typhimurium* strains TA98 (circle) and YG1024 (rhombus). Filled circle and rhombus assayed with S9 mix; open circle and rhombus assayed without S9 mix.

labeling index is a measure of tumor proliferation and reported the association with liver and breast cancer outcome (de Azambuja *et al.*, 2007; Nolte *et al.*, 1998). The increase in Ki-67 index suggested the precancerous status of liver of rats treated by 2,4-DAT (Table 1, Fig. 1). We conclude from these results that genotoxicity assays (i.e., *gpt* and Spi$^-$ assays) and short-term carcinogenicity assays (i.e., GST-P–positive foci formation) can be conducted with F344 *gpt* delta rats. Because we observed genotoxicity in the target organ of carcinogenicity, these results strongly suggest that the carcinogenicity of 2,4-DAT is due to genotoxic activities. Integration of the genotoxicity assay with the pathological assay including GST-P–positive foci formation in *gpt* delta rats could reduce the number of animals necessary for these assays; this would contribute to the adoption of the 3R (reduction, replacement, and refinement) principle for animal use in the life sciences (Balls, 1997). It should be mentioned, however, that GST-P–positive foci formation often needs long treatment periods, for example, 16 and 24 weeks, respectively, for 2-amino-3,8-dimethylimidazo[4,5-*f*]-quinoxaline and 2-acetylaminofluorene (Bagnyukova *et al.*, 2008; Tsuda *et al.*, 2003) and such long treatments may increase the risk of false-positive results of mutations due to nongenotoxic mechanisms caused by chronic toxicity, for example, tumor induction and inflammatory responses (Thybaud et al., 2003).

Why do both 2,6-DAT and 2,4-DAT exhibit mutagenicity *in vitro*? The inconsistency between *in vitro* and *in vivo* results could be due to the different metabolic pathways of 2,6-DAT *in vitro* and *in vivo*. It is plausible that a DAT amino group is first oxidized by a specific cytochrome P450 (e.g., CYP1A2), and the resulting *N*-hydroxy group is further activated by OAT, which leads to the generation of nitrenium ions that can bind to DNA *in vitro* (Watanabe *et al.*, 1994). *In vitro*, both DATs were mutagenic only in the presence of S9 activation, and strain YG1024, which overexpresses OAT, exhibited greater sensitivity to the DATs than did strain TA98 (Fig. 2). Both *S. typhimurium* strains possess GC repetitive sequences in the *hisD* gene that serve as target sites for mutations. We speculate, therefore, that 2,4-DAT could be activated *in vivo* via the pathway described above and induce mostly guanine adducts in DNA. In fact, it was reported that 2,4-DAT induces DNA

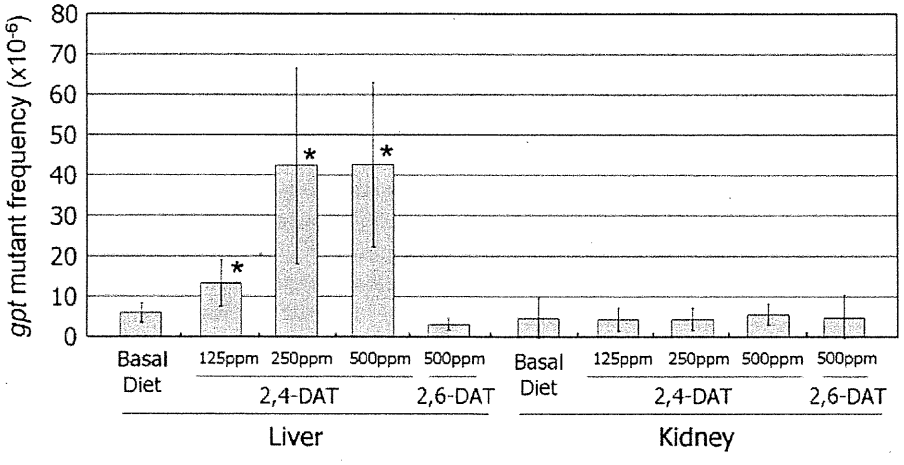

FIG. 3. MFs of *gpt* genes. Values represent mean SD ($n = 5$). Significant differences were observed in 2,4-DAT–treated livers compared to livers from rats fed negative control basal diet. *$p < 0.05$.

TABLE 3
Classification of *gpt* Mutations in *gpt* Delta Rat Livers

Type of gpt Mutation	Basal Diet		125 ppm 2,4-DAT		250 ppm 2,4-DAT		500 ppm 2,4-DAT		500 ppm 2,6-DAT		Basal Diet (DEN)	
	No.	%	No.	%	No.	%	No.	%	No.	%	No.	%
Base substitution												
Transition												
G:C → A:T	4	22	15	26	18	38	12	35	4	27	13	22
(CpG)	(1)		(6)		(6)		(3)		(1)		(3)	
A:T → G:C	1	6	1	2	5	11	1	3	3	20	12	21
Transversion												
G:C → T:A	4	22	16	28	12	26	6	18	4	27	3	5
G:C → C:G	1	6	7	12	4	9	7	21	0	0	0	0
A:T → T:A	0	0	5	9	4	9	1	3	1	7	23	40
A:T → C:G	1	6	4	7	3	6	1	3	0	0	7	12
Deletion												
−1	4	22	3	5	1	2	2	6	1	7	0	0
>2	2	11	2	3	0	0	1	3	2	13	0	0
Insertion	1	6	3	5	0	0	1	3	0	0	0	0
Others	0	0	2	3	0	0	2	6	0	0	0	0
Total	18	100	58	100	47	100	34	100	15	100	58	100

adducts in the livers of rats over 6000 times more efficiently than does 2,6-DAT (Taningher *et al.*, 1995). The sequence analysis that we conducted indicates that most of the mutations induced by 2,4-DAT at 500 ppm were guanine base substitutions; that is, G:C-to-A:T, G:C-to-T:A, and G:C-to-C:G (Table 3). 2,6-DAT might be more efficiently detoxicated than 2,4-DAT *in vivo* because its *para* site at position 4 can be oxidized and subsequently conjugated by phase II enzymes (Cunningham *et al.*, 1989). Detoxication of 2,6-DAT by phase II enzymes may be ineffective *in vitro* compared to *in vivo*. Appropriate cofactors, for example, uridine 5′-diphosphoric acid P2-β-D-glucopyranuronosyl ester for glucuronidation, may be needed to effectively detoxify the active metabolites of 2,6-DAT *in vitro*. At present, however, we cannot rule out the possibility that other factors, such as DNA repair, cell proliferation, translesion DNA synthesis, or apoptosis, might be involved in the differences in mutagenicity of 2,6-DAT *in vitro* and *in vivo*.

TABLE 4
Spi⁻ Mutant Frequency in Rat Livers

Treatment	No. of Rats	Mutant Frequency ($\times 10^{-6}$) (Mean ± SD)	*p* Value (*t*-test)
Basal diet	5	4.43 ± 1.99	
Basal diet (DEN)	5	341.22 ± 180.91	0.002
125 ppm 2,4-DAT	5	8.20 ± 4.75	0.07
250 ppm 2,4-DAT	5	13.42 ± 4.83	0.003
500 ppm 2,4-DAT	5	15.98 ± 4.45	0.0004
500 ppm 2,6-DAT	5	5.49 ± 2.53	0.241

In addition to the discrepancy between *in vitro* and *in vivo* mutagenicity, neither 2,4-DAT nor 2,6-DAT was genotoxic in the bone marrows of rats according to the MN assay (Supplementary table 3). 2,4-DAT is also not mutagenic when applied to MutaMouse skin (Kirkland and Beevers, 2006). Thus, we suggest that the negative results of the MN assay may be due to inefficient metabolic activation of 2,4-DAT at extrahepatic sites. Alternatively, the active metabolites generated in the liver may not reach the bone marrow. The poor metabolic activation in extrahepatic sites and/or short half-lives of the active metabolites may also account for the negative results of the MN assay with DEN in the bone marrow (Supplementary table 3). The MN assay is usually the first choice for *in vivo* genotoxicity assays in the development of pharmaceuticals; our results indicate that rather than relying on the MN assay in the bone marrow, genotoxicity should be evaluated in multiple organs, including the target organs of carcinogenicity.

The Spi⁻ assay is unique to *gpt* delta mice and rats and identifies deletion-type mutations (Nohmi *et al.*, 2000). Previous studies with *gpt* delta mice suggested that genotoxic compounds and physical factors (e.g., radiation) induce different types of deletion mutations *in vivo* (Nohmi and Masumura, 2005). For example, heavy-ion radiation, ultraviolet B radiation, and mitomycin C induce large deletions in the liver, epidermis, and bone marrow, respectively, at molecular sizes of >1 kbp (Horiguchi *et al.*, 2001; Masumura *et al.*, 2002; Takeiri *et al.*, 2003). In contrast, aromatic amines such as 2-amino-1-methyl-6-phenylimidazo[4,5-b]pyridine (PhIP) and aminophenylnorharman (APNH) induce −1 frameshift mutations in runs of guanine bases in the colon and liver, respectively (Masumura *et al.*, 2000, 2003). We characterized Spi⁻ mutants obtained from the livers of rats treated with 500-ppm 2,4-DAT and concluded that, like PhIP and APNH, 2,4-DAT induces mostly −1 frameshift mutations (Supplementary table 5). These results suggest that Spi⁻ assay, as well as the *gpt* assay, is useful for characterizing mutations, which may constitute the molecular basis of chemically induced carcinogenesis.

At the 2006 International Conference on Harmonization of Technical Requirements for Registration of Pharmaceuticals for Human Use meeting held in Yokohama, Japan, revisions of the guidelines for a basic test battery of *in vitro* and *in vivo* genotoxicity tests were discussed (Hayashi, 2008). The current guidelines recommend two *in vitro* assays (Ames test and either a mammalian chromosome aberration test or a mammalian gene mutation test) plus one *in vivo* assay (usually MN test). Because of the high rate of false positives with *in vitro* mammalian cell assays (Kirkland *et al.*, 2005), however, an alternative test battery was proposed at the meeting (Hayashi, 2008). The new battery is composed of one *in vitro* assay (Ames test) plus two *in vivo* assays (MN test plus a second *in vivo* test such as a transgenic assay or *in vivo* comet assay). It is possible to choose the classical battery of two *in vitro* assays plus one

in vivo assay instead of the alternative new battery. With the 3R principle in mind, integration of *in vivo* genotoxicity assays and a 28-day repeated dose toxicity assay was also discussed. *In vivo* mutagenicity assays and an *in vivo* MN assay can be integrated into a 28-day repeated dose toxicity study when transgenic rodents are used (Thybaud *et al.*, 2003). In this study, we found that an *in vivo* genotoxicity assay and a short-term bioassay for liver carcinogenesis using GST-P–positive foci as an end point of preneoplastic lesions can be conducted with F344 *gpt* delta rats. Integration of the two assays using transgenic rats may further facilitate adoption of the 3R principle in regulatory toxicology.

SUPPLEMENTARY DATA

Supplementary data are available online at http://toxsci.oxfordjournals.org/.

FUNDING

Ministry of Education, Culture, Sports, Science and Technology, Japan (18201010); the Ministry of Health, Labour and Welfare, Japan (MHLW; H21-Food-General-009); the Japan Health Science Foundation (KHB1007); MHLW (20 designated-8).

REFERENCES

Aoki, Y., Hashimoto, A. H., Amanuma, K., Matsumoto, M., Hiyoshi, K., Takano, H., Masumura, K., Itoh, K., Nohmi, T., and Yamamoto, M. (2007). Enhanced spontaneous and benzo(a)pyrene-induced mutations in the lung of *Nrf2*-deficient *gpt* delta mice. *Cancer Res.* **67,** 5643–5648.

Bagnyukova, T. V., Tryndyak, V. P., Montgomery, B., Churchwell, M. I., Karpf, A. R., James, S. R., Muskhelishveli, L., Beland, F. A., and Pogribny, I. P. (2008). Genetic and epigenetic changes in rat preneoplastic liver tissue induced by 2-acetylaminofluorene. *Carcinogenesis* **29,** 638–646.

Balls, M. (1997). The three Rs concept of alternatives to animal experimentation. In *Animal Alternatives* (L. F. M. van Zutphen and M. Balls, Eds.), pp. 27–41. Elsevier, Amsterdam.

Cunningham, M. L., Burka, L. T., and Matthews, H. B. (1989). Metabolism, disposition, and mutagenicity of 2,6-diaminotoluene, a mutagenic non-carcinogen. *Drug Metab. Dispos.* **17,** 612–617.

Cunningham, M. L., Hayward, J. J., Shane, B. S., and Tindall, K. R. (1996). Distinction of mutagenic carcinogens from a mutagenic noncarcinogen in the big blue transgenic mouse. *Environ. Health Perspect.* **104**(Suppl. 3), 683–686.

de Azambuja, E., Cardoso, F., de Castro, G., Jr, Colozza, M., Mano, M. S., Durbecq, V., Sotiriou, C., Larsimont, D., Piccart-Gebhart, M. J., and Paesmans, M. (2007). Ki-67 as prognostic marker in early breast caner: a meta-analysis of published studies involving 12,155 patients. *Br. J. Cancer.* **96,** 1504–1513.

Eastmond, D. A., Hartwig, A., Anderson, D., Anwar, W. A., Cimino, M. C., Dobrev, I., Douglas, G. R., Nohmi, T., Phillips, D. H., and Vickers, C. (2009). Mutagenicity testing for chemical risk assessment: update of the WHO/IPCS Harmonized Scheme. *Mutagenesis* **24,** 341–349.

Gerdes, J., Schwab, U., Lemke, H., and Stein, H. (1983). Production of a mouse monoclonal antibody reactive with a human nuclear antigen associated with cell proliferation. *Int. J. Cancer* **31,** 13–20.

Hashimoto, A. H., Amanuma, K., Masumura, K., Nohmi, T., and Aoki, Y. (2009). *In vivo* mutagenesis caused by diesel exhaust in the testis of *gpt* delta mouse. *Genes Environ.* **31,** 1–8.

Hayashi, H., Kondo, H., Masumura, K., Shindo, Y., and Nohmi, T. (2003). Novel transgenic rat for in vivo genotoxicity assays using 6-thioguanine and Spi selection. *Environ. Mol. Mutagen.* **41,** 253–259.

Hayashi, M. (2008). Update on the maintenance of the ICH S2 genetic toxicology. *Pharm. Regul. Sci.* **39,** 515–521.

Heddle, J. A., Dean, S., Nohmi, T., Boerrigter, M., Casciano, D., Douglas, G. R., Glickman, B. W., Gorelick, N. J., Mirsalis, J. C., Martus, H. J., *et al.* (2000). *In vivo* transgenic mutation assays. *Environ. Mol. Mutagen.* **35,** 253–259.

Horiguchi, M., Masumura, K. I., Ikehata, H., Ono, T., Kanke, Y., and Nohmi, T. (2001). Molecular nature of ultraviolet B light-induced deletions in the murine epidermis. *Cancer Res.* **61,** 3913–3918.

Ito, N., Imaida, K., Asamoto, M., and Shirai, T. (2000). Early detection of carcinogenic substances and modifiers in rats. *Mutat. Res.* **462,** 209–217.

Kirkland, D., Aardema, M., Henderson, L., and Muller, L. (2005). Evaluation of the ability of a battery of three *in vitro* genotoxicity tests to discriminate rodent carcinogens and non-carcinogens I. Sensitivity, specificity and relative predictivity. *Mutat. Res.* **584,** 1–256.

Kirkland, D., and Beevers, C. (2006). Induction of *LacZ* mutations in Muta Mouse can distinguish carcinogenic from non-carcinogenic analogues of diaminotoluenes and nitronaphthalenes. *Mutat. Res.* **608,** 88–96.

Kirsch-Volders, M., Aardema, M., and Elhajouji, A. (2000). Concepts of threshold in mutagenesis and carcinogenesis. *Mutat. Res.* **464,** 3–11.

Maron, D. M., and Ames, B. N. (1983). Revised methods for the salmonella mutagenicity test. *Mutat. Res.* **113,** 173–215.

Masumura, K., Matsui, M., Katoh, M., Horiya, N., Ueda, O., Tanabe, H., Yamada, M., Suzuki, H., Sofuni, T., and Nohmi, T. (1999). Spectra of *gpt* mutations in ethylnitrosourea-treated and untreated transgenic mice. *Environ. Mol. Mutagen.* **34,** 1–8.

Masumura, K., Matsui, K., Yamada, M., Horiguchi, M., Ishida, K., Watanabe, M., Wakabayashi, K., and Nohmi, T. (2000). Characterization of mutations induced by 2-amino-1-methyl-6-phenylimidazo[4,5-*b*]pyridine in the colon of *gpt* delta transgenic mouse: novel G: C deletions beside runs of identical bases. *Carcinogenesis* **21,** 2049–2056.

Masumura, K., Kuniya, K., Kurobe, T., Fukuoka, M., Yatagai, F., and Nohmi, T. (2002). Heavy-ion-induced mutations in the *gpt* delta transgenic mouse: comparison of mutation spectra induced by heavy-ion, X-ray, and gamma-ray radiation. *Environ. Mol. Mutagen.* **40,** 207–215.

Masumura, K., Totsuka, Y., Wakabayashi, K., and Nohmi, T. (2003). Potent genotoxicity of aminophenylnorharman, formed from non-mutagenic norharman and aniline, in the liver of *gpt* delta transgenic mouse. *Carcinogenesis* **24,** 1985–1993.

National Toxicology Program. (1979). Bioassay of 2,4-diaminotoluene for possible carcinogenicity. *Natl. Cancer Inst. Carcinog. Tech. Rep. Ser.* **162,** 1–139.

National Toxicology Program. (1980). Bioassay of 2,6-toluenediamine dihydrochloride for possible carcinogenicity (CAS No. 15481-70-6). *Natl. Toxicol. Program Tech. Rep. Ser.* **200,** 1–123.

Nohmi, T. (2008). Possible mechanisms of practical thresholds for genotoxicity. *Genes Environ.* **30,** 108–113.

Nohmi, T., Katoh, M., Suzuki, H., Matsui, M., Yamada, M., Watanabe, M., Suzuki, M., Horiya, N., Ueda, O., Shibuya, T., *et al.* (1996). A new

transgenic mouse mutagenesis test system using Spi and 6-thioguanine selections. *Environ. Mol. Mutagen.* **28,** 465–470.

Nohmi, T., and Masumura, K. (2005). Molecular nature of intrachromosomal deletions and base substitutions induced by environmental mutagens. *Environ. Mol. Mutagen.* **45,** 150–161.

Nohmi, T., Suzuki, T., and Masumura, K. (2000). Recent advances in the protocols of transgenic mouse mutation assays. *Mutat. Res.* **455,** 191–215.

Nolte, M., Werner, M., Nasarek, A., Bektas, H., von Wasielewski, R., Klempnauer, J., and Georgii, A. (1998). Expression of proliferation associated antigens and detection of numerical chromosome aberrations in primary human liver tumors: relevance to tumor characteristic and prognosis. *J. Clin. Pathol.* **51,** 47–51.

Ogiso, T., Tatematsu, M., Tamano, S., Tsuda, H., and Ito, N. (1985). Comparative effects of carcinogens on the induction of placental glutathione S-transferase-positive liver nodules in a short-term assay and of hepatocellular carcinomas in a long-term assay. *Toxicol. Pathol.* **13,** 257–265.

Preston, R. J., and Hoffmann, G. R. (2007). Genetic toxicology. In *Casarett and Doull's Toxicology: The Basic Science of Poisons* (C. D. Klaassen, Ed.), pp. 381–413. The McGraw-Hill Companies, Inc., New York.

Shibata, A., Maeda, D., Ogino, H., Tsutsumi, M., Nohmi, T., Nakagama, H., Sugimura, T., Teraoka, H., and Masutani, M. (2009). Role of Parp-1 in suppressing spontaneous deletion mutation in the liver and brain of mice at adolescence and advanced age. *Mutat. Res.* **664,** 20–27.

Takeiri, A., Mishima, M., Tanaka, K., Shioda, A., Ueda, O., Suzuki, H., Inoue, M., Masumura, K., and Nohmi, T. (2003). Molecular characterization of mitomycin C-induced large deletions and tandem-base substitutions in the bone marrow of *gpt* delta transgenic mice. *Chem. Res. Toxicol.* **16,** 171–179.

Taningher, M., Peluso, M., Parodi, S., Ledda-Columbano, G. M., and Columbano, A. (1995). Genotoxic and non-genotoxic activities of 2,4- and 2,6-diaminotoluene, as evaluated in Fischer-344 rat liver. *Toxicology* **99,** 1–10.

Thybaud, V., Dean, S., Nohmi, T., de Boer, J., Douglas, G. R., Glickman, B. W., Gorelick, N. J., Heddle, J. A., Heflich, R. H., Lambert, I., *et al.* (2003). *In vivo* transgenic mutation assays. *Mutat. Res.* **540,** 141–151.

Tsuda, H., Fukushima, S., Wanibuchi, H., Morimura, K., Nakae, D., Imaida, K., Tatematsu, M., Hirose, M., Wakabayashi, K., and Moore, M. A. (2003). Value of GST-P positive preneoplastic hepatic foci in dose-response studies of hepatocarcinogenesis: evidence for practical thresholds with both genotoxic and nongenotoxic carcinogens. A review of recent work. *Toxicol. Pathol.* **31,** 80–86.

Umemura, T., Kanki, K., Kuroiwa, Y., Ishii, Y., Okano, K., Nohmi, T., Nishikawa, A., and Hirose, M. (2006). *In vivo* mutagenicity and initiation following oxidative DNA lesion in the kidneys of rats given potassium bromate. *Cancer Sci.* **97,** 829–835.

Umemura, T., Tasaki, M., Kijima, A., Okamura, T., Inoue, T., Ishii, Y., Suzuki, Y., Masui, N., Nohmi, T., and Nishikawa, A. (2009). Possible participation of oxidative stress in causation of cell proliferation and *in vivo* mutagenicity in kidneys of *gpt* delta rats treated with potassium bromate. *Toxicology* **257,** 46–52.

Watanabe, M., Igarashi, T., Kaminuma, T., Sofuni, T., and Nohmi, T. (1994). N-hydroxyarylamine *O*-acetyltransferase of Salmonella typhimurium: proposal for a common catalytic mechanism of arylamine acetyltransferase enzymes. *Environ. Health Perspect.* **102**(Suppl. 6), 83–89.

Xu, A., Smilenov, L. B., He, P., Masumura, K., Nohmi, T., Yu, Z., and Hei, T. K. (2007). New insight into intrachromosomal deletions induced by chrysotile in the *gpt* delta transgenic mutation assay. *Environ. Health Perspect.* **115,** 87–92.